Promotional effect of H_2O introduction on the NH_3-SCR activity of the gas-phase sulfated CeO_2 catalyst by organic CS_2+COS: Influence of H_2O concentration

Jiaxing Liu[1], Yafei Zhu[1], Zhenchang Sun[1], Yanping Du[2], Zhibo Xiong[1*], Fei Zhou[3], Jing Jin[1], Qiguo Yang[1], Wei Lu[1]

1. School of Energy and Power Engineering, University of Shanghai for Science & Technology, Shanghai, 200093, China

2. School of Engineering, Lancaster University, Lancaster, LA1 4YW, UK

3. Jiangsu Guoxin Jingjiang Power Co. Ltd., Jingjiang 214500, Jiangsu, China

Abstract: Herein, as an indispensable key reactant for the hydrolysis of organic sulfur, H_2O was firstly introduced to optimize the NH_3-SCR activity of CeO_2 by providing the adsorption and reaction spots of catalysis for organic CS_2+COS during the low-temperature gas-phase sulfation. The results demonstrate that the introduction of 0.33 vol.% H_2O is beneficial to enhance the interaction between organic CS_2+COS and cube fluorite CeO_2, which not only increases the concentrations of Ce^{3+} ions, chemisorbed oxygen (O_β) and oxygen vacancies on CeO_2-CS_2+COS surface, but also effectively enhances the redox cycle of Ce^{4+}/Ce^{3+} ion pairs and the medium-strong acid sites of catalyst. These all help enhance the promotional effect of organic sulfur low-temperature gas-phase sulfation on the NH_3-SCR activity of CeO_2 and further improve NO_x reduction over the CeO_2-CS_2+COS catalyst. However, the introduction of 5.0 vol.% H_2O shows a certain inhibitory effect due to the competitive adsorption of excess water and COS+CS_2 on the cube fluorite CeO_2 surface, which weakens their interaction during the low-temperature gas-phase sulfation, thereby decreases the promotional effect of low concentration water introduction on the NH_3-SCR activity of the CeO_2-CS_2+COS catalyst. Therefore, the results of this research provide a scientific reference for developing the NH_3-SCR CeO_2-based catalyst in practical applications.

Keywords: NH_3-SCR, CeO_2, Organic sulfur, Low-temperature gas-phase sulfation, H_2O concentration

* Corresponding author: Zhibo Xiong, Tel.: +86 21 55272320, Email addresses: xzb412@usst.edu.cn (Z.Xiong)

1. Introduction

The rapid development of global economy inevitably leads to an intense demand of energy or/and fuel, thus the traditional fossil fuels (coal, oil, and natural gas, etc.) have been extensively utilized in power generation, transportation and industry [1-3]. However, large fine particulate matter (PM 2.5) and greenhouse gases (CO_2, CH_4, etc.) are discharged during the utilization of fossil fuels and 3 million tons of CO_2 can be emitted for a 500MW coal-fired power plants per year, and the concentration of CO_2 in the atmosphere is expected to exceed 500 ppm by 2050 [4,5]. In addition, the toxic and harmful gases such as nitrogen oxides (NO_x, mainly NO and NO_2) and sulfur-containing compounds (SO_2, COS, CS_2, etc.) are also produced during the combustion of fossil fuels, which brings many environmental problems [6,7]. For example, the emission of nitrogen oxides and sulfur compounds are prone to oxidation reactions, causing acid rain, photochemical smog, ozone holes and other environmental disasters [8-10]. Therefore, it is necessary to develop an effective method to reduce nitrogen oxide and sulfur compounds.

Compared to inorganic SO_2, organic carbonyl sulfide (COS) and carbon disulfide (CS_2) are linear triatomic molecules similar to carbon dioxide (CO_2), which are less reactive and difficult to be removed [11,12]. At present, catalytic hydrolysis [13,14], hydrogenation [15,16], adsorption and absorption [17-19] have been developed to reduce the emission of organic sulfur. Among them, catalytic hydrolysis has the advantages of low energy consumption, less side reactions and high efficiency, especially when dealing with high levels of organic sulfur. Wang et al. found that the synthesized (Co+Ni)/Al catalyst derived from various hydrotalcite-like compounds presented a good catalytic hydrolysis activity of COS, and the introduction of Ce additive effectively improved its catalytic performance due to the alterations of the structural properties, oxidation properties and surface defect sites [20,21]. At present, the development of the low temperature hydrolysis catalyst to reduce organic sulfur has attracted widespread attention, especially the metal oxide catalysts with a rich pore structure, a good thermal stability, abundant basic sites and a strong anti-poisoning ability. For instance, the introduction of 3DOM structure via the colloidal crystal template method is beneficial to the extraction of the hydrolysis product H_2S from the aluminum-based and titanium-based hydrolysis catalysts, inhibiting the

deposition of sulfate species on catalysts surface [22].

Generally, the hydrolysis of organic sulfur is an alkali-catalyzed reaction process: H_2O firstly adsorbs and dissociates on metal oxides surface to form -OH groups, and then CS_2 preferentially adsorbs on the surface basic sites of catalyst and generates thiocarbonate ($HSCO_2^-$) or COS intermediates via the interaction of -OH group and M-O pair (M: Ti, Al, Fe, Ce, etc.). Subsequently, the formed COS can further be converted into $HSCO_2^-$ through the above hydrolysis reaction pathway, and the intermediate of $HSCO_2^-$ finally decomposes into CO_2 and H_2S under the action of -OH group and M-O pair to complete the catalytic hydrolysis of organic sulfur [23-27]. Therefore, the surface basic sites of catalyst play a dominant role on the hydrolysis activity of organic sulfur. It should be noted that the active -OH groups on the catalyst surface can serve as an alkaline site for the adsorption and activation of organic sulfur, thus promotes the hydrolysis reaction. A large number of literatures had also investigated the effect of H_2O on the hydrolysis efficiency of organic sulfur. Gao et al. [28] pointed out that the absorbed H_2O could dissociate into generate active -OH groups for the hydrolysis reaction of COS on catalyst surfaces, thus ensured the stable and efficient hydrolysis of organic sulfur. Wang et al. [29] found that the presence of H_2O on the alumina catalyst surface slowed down the deactivation process of organic sulfur hydrolysis by promoting the deposition and adsorption of sulfur and sulfate species at different sites. It is worth noting that the presence of H_2O also has a negative effect on the hydrolysis removal of COS/CS_2. Gu et al. [25] reported that the excessive H_2O on catalyst surface led to a competitive adsorption with COS, which inhibited the hydrolysis reaction and reduced the COS removal efficiency. This phenomenon had also been found in the hydrolysis process of CS_2 [30]. Furthermore, the presence of H_2O could promote the formation of sulfur-containing species (sulfates), which had been considered to be the main reason for the deactivation of organic sulfur hydrolysis for catalysis [26]. Because the accumulation of sulfur-containing species on the catalyst surface led to the blockage of pore structure, and also reduced the basic sites of catalyst due to the formation of surface sulfates, resulting in the deactivation of organic sulfur hydrolysis [23,31]. Therefore, H_2O plays an essential role in the formation of sulfur-containing species during the hydrolysis process of organic sulfur.

Owing to the unique 4f electronic structure, CeO_2 presents an excellent oxygen storage capacity (OSC) and redox ability [32], which has been used as the main active components or

doping additives in the selective catalytic reduction of NO_x with NH_3 (NH_3-SCR). However, pure CeO_2 exhibits bad NH_3-SCR performance due to the poor surface acidity and NH_3 peroxidation at high temperatures, which limits its application in engineering. Interestingly, the formed surface sulfates during the hydrolysis of organic sulfur might retain Lewis acid sites and enhance Brønsted acid sites of CeO_2, thus contributes to the adsorption and activation of NH_3 on it surface [33,34]. Actually, the formed sulfate species can serve as the reducible species to promote redox reactions and improve the NH_3-SCR activity of cerium-based catalysts [35,36]. Therefore, the sulfation treatment, including the gas-phase sulfation of the traditional SO_2 and the liquid-phase sulfation of H_2SO_4/$(NH_4)_2SO_4$/$CS(NH_2)_2$, have been regarded as the effective strategy to improve the de-nitrification activity of cerium-based catalysts mainly via optimizing the surface acidity [37-42]. Our previous study [33] showed that the gas-phased sulfation of organic sulfur (CS_2 or COS) at 300 °C presented a better improvement on the NH_3-SCR activity of CeO_2 than the traditional SO_2. Recently, we have found that the gas-phased sulfation of CS_2 or/and COS under the low-temperature hydrolysis conditions can further improve the catalytic performance of NO_x reduction over the CeO_2 catalyst. The above references indicated that the presence of H_2O contributed to regulating the formation of sulfur-containing species on the catalyst surface during the low-temperature hydrolysis process, thus might affect the surface acidity of the used cerium-based catalyst, which had been widely proven to improve the NH_3-SCR activity of CeO_2. However, the promotional effect of low-temperature hydrolysis of organic CS_2 or/and COS on the NH_3-SCR activity of CeO_2 catalyst has rarely been studied, especially under the presence of H_2O.

Furthermore, H_2O widely co-present with organic sulfur in blast furnace gas, which can affect the hydrolysis of CS_2 or/and COS over catalysts. Meanwhile, cerium oxide had been verified to improve the anti-oxygen poisoning of catalyst for the hydrolysis of organic sulfur by avoiding the sulfation of active species due to its better adsorption of sulfates [21,24]. Therefore, as an indispensable key reactant for the hydrolysis of organic sulfur, H_2O is proposed for the first time to improve the NH_3-SCR catalytic activity of CeO_2 during the low-temperature gas-phase sulfation of organic CS_2 and COS, which is more conducive to the synthesis of catalysts with excellent performance in practical engineering. The results demonstrate that the introduction of H_2O further enhances the promotional effect of CS_2+COS gas-phase sulfation on the NH_3-SCR

activity of CeO_2 catalyst at the simulated low-temperature for the hydrolysis of organic sulfur. Furthermore, a series of characterization techniques were employed to investigate the sulfuric acid optimized strategy of the "CS_2+COS+H_2O" gas-phase sulfation on the physicochemical properties, reduction properties, sulfate species, and NH_3-SCR performance of CeO_2.

2. Experimental

2.1. Catalyst preparation

Pure CeO_2 was synthesized via a one-pot hydrothermal method [33,43], and the used cerium nitrate ($Ce(NO_3)_3 \cdot 6H_2O$, AR), ammonium bicarbonate (NH_4HCO_3, AR) and hydrogen peroxide (H_2O_2, AR) were purchased from China Pharmaceutical Group Chemical Reagents Co., Ltd. According to the preparation of CeO_2 in Scheme 1, 0.005 mol $Ce(NO_3)_3 \cdot 6H_2O$ was firstly dissolved in deionized water and stirred violently for 2 hours until a clear and transparent solution was obtained. Next, a certain amount of ammonium bicarbonate was added into the mixed solution with a milky white suspension formed. After being stirred for 30 minutes, 9 mL of H_2O_2 (10 mol/L) was dropped and the milky white solution quickly turned into orange. Finally, the mixed solution was poured into a 100 mL of polytetrafluoroethylene and transferred to stainless steel autoclave. After being hydrothermally heated at 200 °C for 24 hours, the resulting precipitate was washed with deionized water and anhydrous ethanol until the pH reached 7. The obtained precipitate was dried at 80 °C for 12 hours and calcined at 400 °C for 5 hours in a temperature-programmed muffle furnace to obtain pure CeO_2 catalyst.

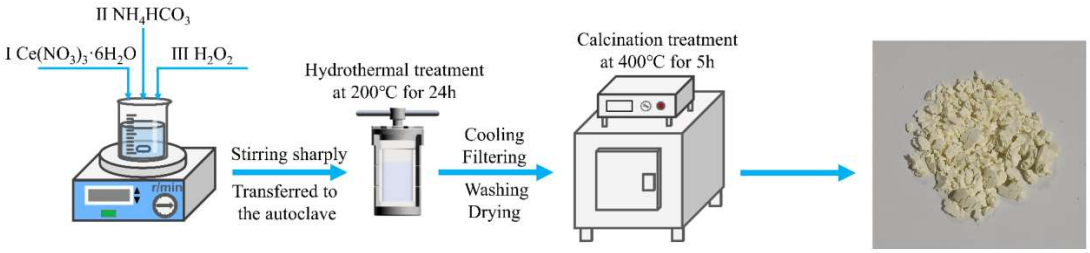

Scheme 1. Schematic diagram for the preparation of pure CeO_2 by the one-pot hydrothermal method.

The gas phase sulfation of CeO_2 was carried out in a tube furnace according to the following sulfation conditions (Scheme 2): the total gas flow rate of the simulated COS and CS_2 (the molar ratio of 7:3) is 500 mL/min by ensuring the concentration of S element being 200 ppm [33]. A certain concentration of H_2O was introduced into the vulcanization test bench via an injection pump and N_2 was used as the equilibrium gas. The gas-phase sulfation was carried out

at 50 °C for 3 hours. For convenience, the pretreated samples were labeled as CeO_2-CS_2+COS without water, CeO_2-CS_2+COS-H_2O(x), where x represents the concentration of water (x = 0.33%, 1.5%, 5.0%).

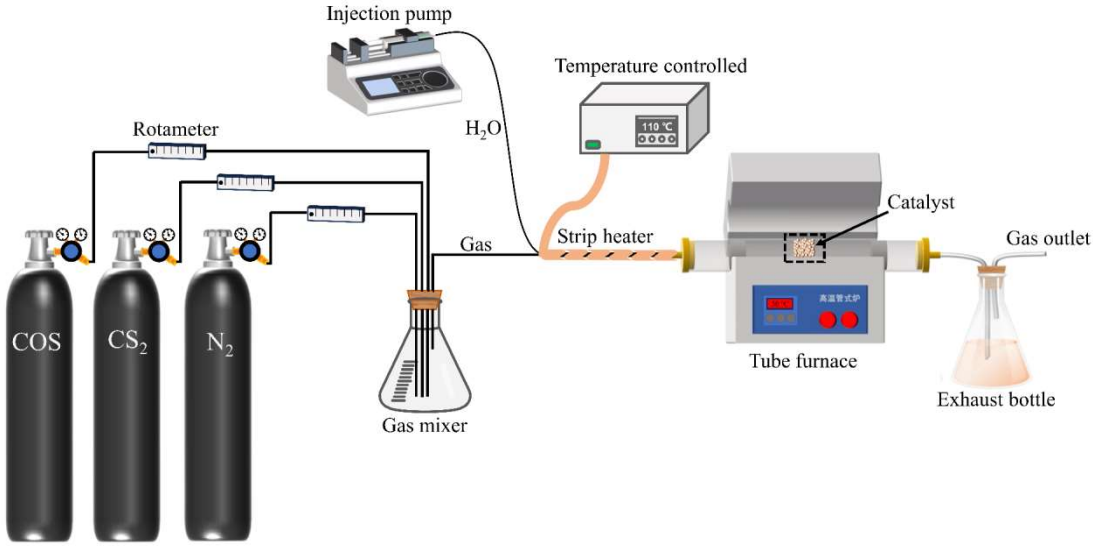

Scheme 2. The low temperature gas-phase sulfation of CeO_2 catalyst by organic sulfur.

2.2. Catalytic activity test

The fixed bed reactor was used to test the NH_3-SCR catalytic performance of catalysts. The dosage of sample and the total gas flow rate are 0.45 g (40~60 mesh) and 1500 mL/min with the gas hourly space velocity (GHSV) being 200,000 mL/(g·h). The flue gas reaction conditions are as follows: 600 ppm NH_3, 600 ppm NO, 5 vol.% O_2 and 99.999 vol.% N_2 used as the equilibrium gases. The concentration of inlet and outlet flue gas (O_2, NO_x) was continuously monitored by T-350 flue gas analyzer (Testo, Germany). Then, the NO_x conversion rate (η) is calculated according to the following formula: $\eta = (1-[NO_x]_{out}/[NO_x]_{in})\times 100\%$, where $[NO_x]_{in}$ and $[NO_x]_{out}$ represent the inlet and outlet concentrations of gaseous NO_x (NO and NO_2), respectively.

2.3. Catalyst characterizations

The surface morphology and structure of catalyst were observed through scanning electron microscopy (SEM) using the ZEISS SIGMA HD instrument. The N_2 adsorption-desorption curves were measured at -196 °C using a powder technology ASAP 2460 system instrument. The specific surface area was calculated through the Brunauer-Emmett-Teller (BET) method, while

the Barrett Joyner-Halenda (BJH) method was used to determine the pore volume and pore size distribution. X-ray diffraction (XRD) patterns were obtained using Cu Kα radiation on a 6100 X-ray diffractometer (Rigaku, Japan) at a scanning rate of 5 °/min from 2θ=10 ° to 80 ° and the composition of the diffraction peaks was analyzed using MDI Jade 6.0. Raman spectra of samples were collected on a Raman spectrometer (InVia Reflex, Renishaw), where a laser with a wavelength of 532 nm was used as the excitation source. Fourier transform infrared (FTIR) spectra ranging from 400 to 4000 cm^{-1} were recorded using a Nicolet iS5 FTIR spectrometer, with a resolution of approximately 4 cm^{-1}.

The X-ray photoelectron spectrometer (XPS, Thermo Fisher Scientific Escalab 250 Xi) utilizes Al Kα radiation with an excitation energy of 1486.7 eV. The photoelectron spectroscopy was calibrated with the C1s signal with a binding energy of 284.8 eV and the spectrum was fitted with the Gaussian-Lorentz function using XPSPEAK software. H_2-temperature programmed reduction (H_2-TPR) and NH_3-temperature programmed desorption (NH_3-TPD) analyses were performed using the AutoChem II 2920 instrument from Micromeritics, along with a thermal conductivity detector (TCD). In the H_2-TPR detection process, 100 mg samples were pretreated in an Ar atmosphere at 300 °C for 30 minutes, and then cooled to room temperature. The TPR curves were obtained using a heating rate of 10 °C/min, ranging from 50 to 900 °C in a 10% H_2/Ar flow. For NH_3-TPD analysis, 100 mg samples were subjected to heating at 500°C for an hour in the presence of Ar flow and then cooled to 35°C. A continuous flow of 10% NH_3/He (50 mL/min) was directed through the sample tube for a purge time of 2 hours and the desorption of NH_3 species was carried out in a helium flow to obtained the data at temperatures ranging from 35 to 900 °C. Thermogravimetric analysis (TGA) was conducted using PerkinElmer STA6000 in an α-Al_2O_3 crucible under a nitrogen atmosphere. Thermogravimetric curves in the temperature range of 30-900 °C were recorded with a heating rate of 10 °C/min to investigate the thermal properties and thermal decomposition of the sulfated samples.

3. Results and discussion

3.1. Evaluation of catalytic activity

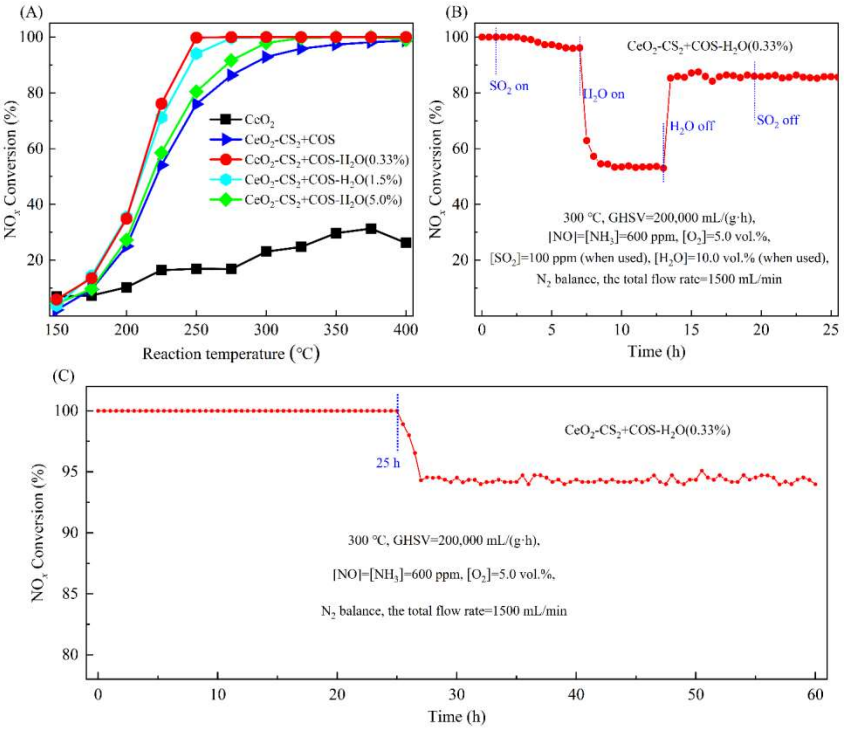

Fig. 1. (A) The effect of H_2O concentration on the NH_3-SCR activity of CeO_2 during the gas-phase sulfation process. Sulfated conditions: $COS:CS_2$ = 7:3 with the total amount of S element being 200 ppm; the sulfation temperature 50 °C; the sulfation time 3 h; H_2O (water vapor) concentrations 0.33 vol.%, 1.5 vol.% and 5.0 vol.%. (B) H_2O and SO_2 resistance study of CeO_2-CS_2+COS-H_2O(0.33%) catalyst and (C) the long time stability test of CeO_2-CS_2+COS-H_2O(0.33%) catalyst.

The influence of H_2O introduction on the NH_3-SCR activity of CeO_2-CS_2+COS catalyst was investigated during the gas-phase sulfation at 50 °C, and the results are given in Fig. 1(A). It can be found that the gas-phase sulfation of COS+CS_2 at 50 °C effectively enhances the NH_3-SCR activity of CeO_2, and the highest NO_x conversion of catalyst is increased from 31% to higher than 90% at the GHSV of 200,000 mL/(g·h). The main reason for the poor catalytic performance of CeO_2 might be attributed to the low concentrations of Ce^{3+} ions, active oxygen and acid sites on its surface [44,45]. And the low-temperature gas-phase sulfation of COS and CS_2 optimizes these defects and improves the surface concentrations of Ce^{3+} ions, active oxygen and acid sites of CeO_2, thereby increases its NH_3-SCR activity effectively. This promotional effect of organic sulfur gas-phase sulfation had also been verified by our previous research [33], and COS or CS_2 presented a better enhancement on the NH_3-SCR activity of CeO_2 than the traditional inorganic SO_2 when the gas-phase sulfation was carried out at 300 °C. Interestingly, as depicted in Fig. 1(A), the introduction of H_2O during the low-temperature gas-phase sulfation of COS and CS_2

can further increase the NH_3-SCR activity of the CeO_2+CS_2+COS catalyst, and CeO_2-CS_2+COS-H_2O(0.33%) presents good catalytic performance with a 100% NO_x reduction obtained at the temperature range of 250 ~ 400 ºC. However, the enhancement of water concentrations from 0.33 vol.% to 5.0 vol.% decreases this promotional effect. In order to validate the disadvantageous effect of high H_2O concentration during the low-temperature gas-phase sulfation, 1.5 vol.% H_2O had also been introduced and the NH_3-SCR activity of CeO_2-CS_2+COS-H_2O(1.5%) is between the values of CeO_2-CS_2+COS-H_2O(0.33%) and CeO_2-CS_2+COS-H_2O(5.0%). This implies that the introduction of H_2O during the low-temperature gas-phase sulfation can optimize the catalytic performance of CeO_2+CS_2+COS catalyst, but large concentration of water decreases this promotional effect. The previous researches about the sulfated CeO_2 and other metals catalyst for NH_3-SCR had been summarized in Table S1, and it can be found that compared to other sulfated catalysts in recent years, CeO_2-CS_2+COS-H_2O(0.33%) exhibits excellent low-temperature performance and a wide temperature window even at a high GHSV of 200,000 mL/(g·h). Meanwhile, the influence of CS_2/COS molar ratio (7:3, 5:5, 3:7) on the NH_3-SCR activity of CeO_2-CS_2+COS-H_2O(0.33%) catalyst was also examined, as shown in Fig. S1. Under the CS_2/COS molar ratios of 7:3 and 3:7, the sulfated CeO_2-CS_2+COS-H_2O(0.33%) catalysts present similar denitrification performance, which are better than that of the catalyst treated at the CS_2/COS molar ratio of 5:5. Meanwhile, it is generally believed that the organic sulfur in blast furnace gas is mainly composed of COS and the molar ratio of COS/(COS+CS_2) is about 70% [24]. Therefore, 7:3 of COS/CS_2 molar ratios was chosen for the subsequent research and characterization.

H_2O and SO_2 that commonly present in the denitrification process and potentially influence the NH_3-SCR activity of catalyst, therefore it is necessary to study the anti-poisoning of H_2O or/and SO_2 for the CeO_2-CS_2+COS-H_2O(0.33%) catalyst. As shown in Fig. 1(B), when 100 ppm SO_2 is introduced into the simulated flue gas, the NO_x reduction of catalyst slowly decreases to 93% and then remains stable, and CeO_2-CS_2+COS-H_2O(0.33%) exhibits excellent resistance to SO_2 poisoning. When further introducing 10.0 vol.% H_2O, the NO_x conversion rate of CeO_2-CS_2+COS-H_2O(0.33%) rapidly decreases to 53%, which might be due to the competitive adsorption of H_2O and the deposition of sulfate species [39,40]. After removing H_2O, the activity is promptly recovered to 85%, which indicates that the catalyst deactivation caused by H_2O is

reversible. After further stopping the introduction of SO_2, the activity is not further recovered, indicating an irreversible deactivation of catalyst caused by the deposition of sulfate species. In the meantime, the long-term stability of the NH_3-SCR activity over the CeO_2-CS_2+COS-H_2O(0.33%) catalyst was also investigated and the results are given in Fig. 1(C). It is found that CeO_2-CS_2+COS-H_2O(0.33%) presents a good stability of the NH_3-SCR activity, and more than 90% of NO_x reduction can be maintained after a 60 h test, although its NO_x reduction decreases from 100% to about 95% at 25~27 h.

Previous studies had shown that an appropriate amount of H_2O could promote the hydrolysis and conversion of organic sulfur (CS_2 or/and COS) via optimizing the formation of active -OH groups on catalysts surface, but excessive H_2O inhibited the catalytic hydrolysis due to the competitive adsorption and the introduced concentration of H_2O could regulate the formation of sulfur-containing species on the catalyst surface during the low-temperature hydrolysis of CS_2 or/and COS [29,46]. Meanwhile, the formed sulfur-containing species, mainly sulfate, were proven to optimize the concentrations of Ce^{3+} ions, active oxygen and acid sites on CeO_2 catalyst surface, which are closely related to its NH_3-SCR activity. Therefore, CeO_2-CS_2+COS-H_2O(0.33%) and CeO_2-CS_2+COS-H_2O(5.0%) were chosen to be characterized to investigate the influence of H_2O introduction on the physical-chemical properties of CeO_2-CS_2+COS catalyst in the following sections.

3.2. Morphological analysis

Scanning electron microscopy (SEM) was applied to investigate the influence of H_2O introduction on the morphology of CeO_2 catalyst during the low-temperature gas-phase sulfation of organic CS_2 and COS, and the particle size distributions were also calculated. According to the results in Fig. 2 and 3. CeO_2 presents an irregular morphology composed of dispersed nanoparticles and exhibits a maximum particle size of 2.33 μm. Meanwhile, the low-temperature gas-phase sulfation of CS_2 and COS decreases the crystallinity of nanoparticles on CeO_2 surface and inhibits the occurrence of agglomeration, although CeO_2-CS_2+COS also exhibits a disordered granular morphology. Furthermore, the introduction of H_2O seems to further reduce the agglomeration of surface nanoparticles and causes the particle size to shift towards smaller direction. In particular, the introduction of 5.0 vol.% H_2O significantly enhances the dispersion of CeO_2 nanoparticles and reduces the average particle size to 0.281 μm. Therefore, the

gas-phase sulfation of organic sulfur at 50 °C decreases the crystallinity of nanoparticles on CeO_2 surface due to the formation of surface sulfur-containing species, and the introduction of H_2O further improves the dispersion of nanoparticles on catalysts surface. Furthermore, the nanoparticles on CeO_2-CS_2+COS-H_2O(5.0%) surface are more evenly dispersed (Fig. 2(D), Fig. 3(D), Fig. S2(D)), which might be due to the inhibition of excess H_2O on the aggregation of sulfate species during the low-temperature gas-phase sulfation of CS_2 and COS.

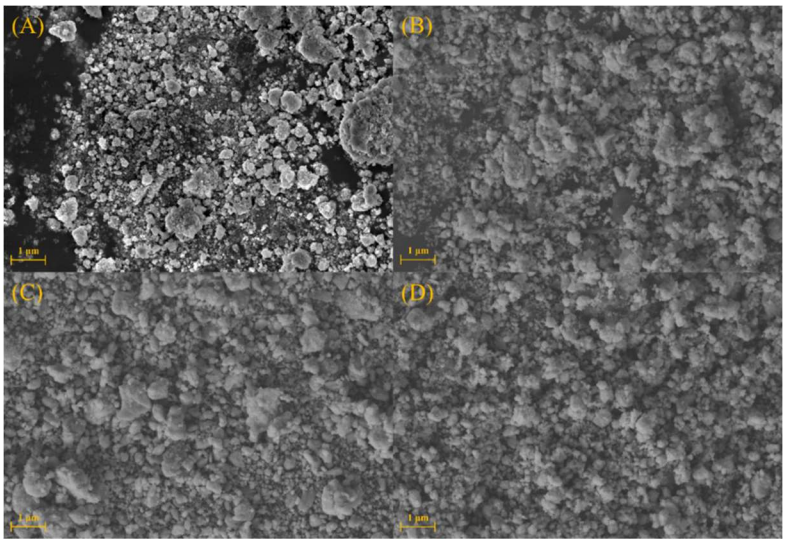

Fig. 2. SEM images of (A) CeO_2, (B) CeO_2-CS_2+COS, (C) CeO_2-CS_2+COS-H_2O(0.33%) and (D) CeO_2-CS_2+COS-H_2O(5.0%) catalysts.

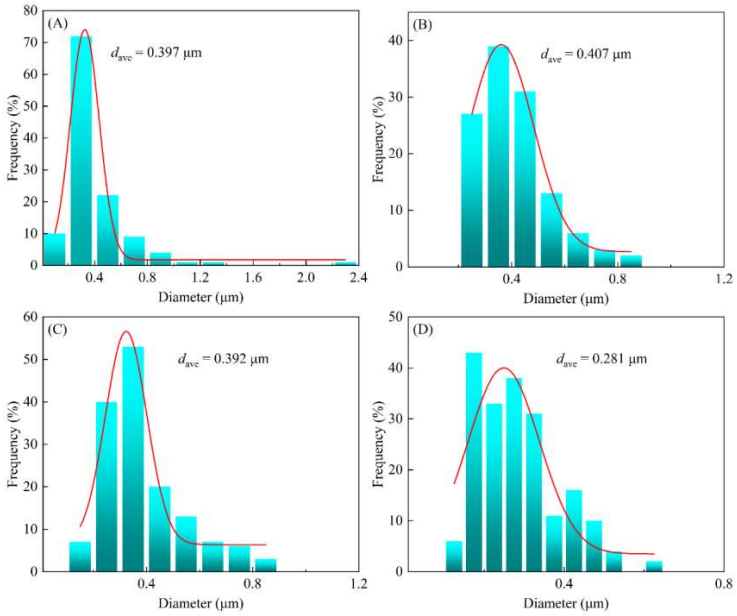

Fig. 3. Particle size distributions of (A) CeO_2, (B) CeO_2-CS_2+COS, (C) CeO_2-CS_2+COS-H_2O(0.33%) and (D) CeO_2-CS_2+COS-H_2O(5.0%) catalysts.

3.3. Texture and structure characterization

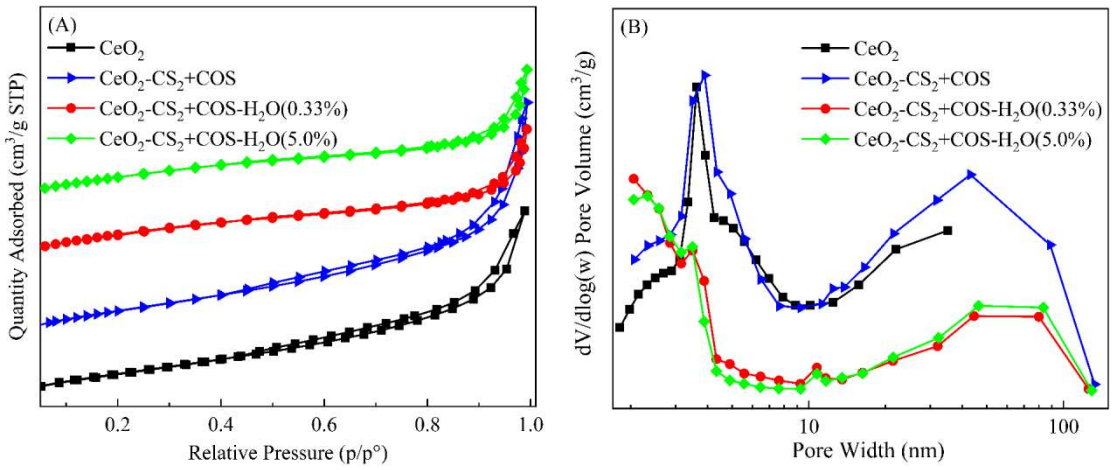

Fig. 4. The N_2 adsorption-desorption isotherms (A) and the pore size distributions (B) of the as-prepared catalysts.

Herein, N_2 adsorption-desorption, XRD and Raman were carried out to reveal the influence of H_2O introduction on the texture and structural properties of the sulfated CeO_2 catalysts by CS_2 and COS at 50 °C. As shown in Fig. 4(A), the adsorption-desorption isotherms of CeO_2 and CeO_2-CS_2+COS catalysts belong to type IV with the hysteresis loop of H3 type in the relative pressure range of p/p° = 0.05~1.0 according to the IUPAC classification, indicating the presence of mesoporous structures composed of non-rigid aggregates of nanoparticles [47,48]. In addition, the rapid increase in nitrogen adsorption capacity at the p/p° of 0.8 demonstrates the presence of a macroporous structure [22,49]. Thus, both CeO_2 and CeO_2-CS_2+COS catalysts have mesoporous and macroporous hierarchical porous structures, which is confirmed by the BJH desorption pore size distribution calculated from the desorption isotherm of N_2. From Fig. 4(B), it can be observed that CeO_2 has a narrow and sharp single peak in the range of 2-10 nm belonging to the typical mesoporous structure, and the gas-phase sulfation of CS_2 and COS at 50 °C widens the pore size distribution of CeO_2. However, the introduction of H_2O during the gas-phase sulfation makes the low-pressure closure point of nitrogen adsorption and desorption for CeO_2-CS_2+COS shift to the right, and both CeO_2-CS_2+COS-H_2O(0.33%) and CeO_2-CS_2+COS-H_2O(5.0%) present more concentrated pore size distribution than CeO_2 and CeO_2-CS_2+COS although they also exhibit the mesoporous and macroporous hierarchical porous structures. This indicates that the presence of water might affect the sulfation degree of nanoparticles and the formation of sulfur-containing species on CeO_2-CS_2+COS surface during the gas-phase sulfation of CS_2 and COS at 50 °C, which are in accordance with the results of the

morphology. Previous studies had pointed out that an abundance of mesopores could provide more active sites and internal surface area for the NH_3-SCR reaction over P-W/CeO_2, and the hierarchical porous structure helped to reduce the mass transfer resistance and facilitated the contact between the reactant gas molecules and the active sites on the inner surface of catalyst [50,51]. Therefore, CeO_2-CS_2+COS-H_2O(0.33%) and CeO_2-CS_2+COS-H_2O(5.0%) exhibit slightly worse mesoporous and macroporous hierarchical porous structures than CeO_2 and CeO_2-CS_2+COS. In addition, they have smaller specific surface areas (Table 1). These all demonstrate that the introduction of H_2O affect the sulfation degree of nanoparticles and the accumulation of the formed sulfur-containing species during the gas-phase sulfation of CS_2 and COS at 50 °C, but the pore structure and specific surface area might not be the determining factor for the NH_3-SCR activity of the sulfated CeO_2 catalysts by organic sulfur at low-temperatures.

Table 1 The physical structural parameters of the as-prepared catalysts

Samples	BET surface area [a] (m^2/g)	Pore volume [b] (cm^3/g)	Pore diameter [c] (nm)
CeO_2	119.62	0.199	6.44
CeO_2-CS_2+COS	127.86	0.280	8.34
CeO_2-CS_2+COS-H_2O(0.33%)	113.31	0.155	6.43
CeO_2-CS_2+COS-H_2O(5.0%)	107.25	0.156	6.71

[a] BET surface area

[b] BJH desorption pore volume

[c] BJH desorption pore diameter

According to the X-ray diffraction (XRD) patterns in Fig. 5 and Fig. S3, pure CeO_2 presents the typical lattice diffraction peaks attributed to cubic fluorite CeO_2 (PDF#34-0394) [40,52], and the low-temperature gas-phase sulfation of CS_2 and COS effectively reduces the intensity of the diffraction peaks ascribed to cubic fluorite CeO_2. Furthermore, a broad peak at the low scanning angle range of 15 ~ 26 ° appears over the CeO_2-CS_2+COS catalyst, which is attributed to the sulfur elements or/and the sulfur compounds dominated by hydrated metal sulfates (PDF#37-0762; PDF#24-1250; PDF#24-1216). Interestingly, the introduction of 0.33 vol.% H_2O might slightly suppress the sulfation of cubic fluorite CeO_2 by CS_2 and COS at 50 °C, but

CeO_2-CS_2+COS-H_2O(0.33%) still presents a similar broad peak of sulfur elements or/and compounds to CeO_2-CS_2+COS. However, the enhancement of H_2O concentration from 0.33 vol.% to 5.0 vol.% increases the intensity of this peak, indicating that higher crystallinity sulfur elements or/and compounds are formed in CeO_2-CS_2+COS-H_2O(5.0%). Mu et al. [53] pointed out that the hydrolysis of COS led to a new XRD pattern peak emerging at 2θ = 24.2 ° in 10Cu-Co_3O_4 catalyst, which was attributed to elemental sulfur. This phenomenon was also found in the CeO_2-R catalyst after the catalytic selective oxidation of H_2S [54]. In addition, the hydrated metal sulfates could gradually become amorphous during the slow heating process, which further thermally decomposed into the anhydrous sulfate species such as $Ce_2(SO_4)_3$ and $Ce(SO_4)_2$ [55]. Therefore, the low-temperature gas-phase sulfation of organic CS_2+COS contributes to the formation of sulfur element or/and compounds in the CeO_2 catalyst under the condition of low concentration water, but the enhancement of H_2O concentration from 0.33 vol.% to 5.0 vol.% further improves the crystallinity of the formed sulfur-containing species.

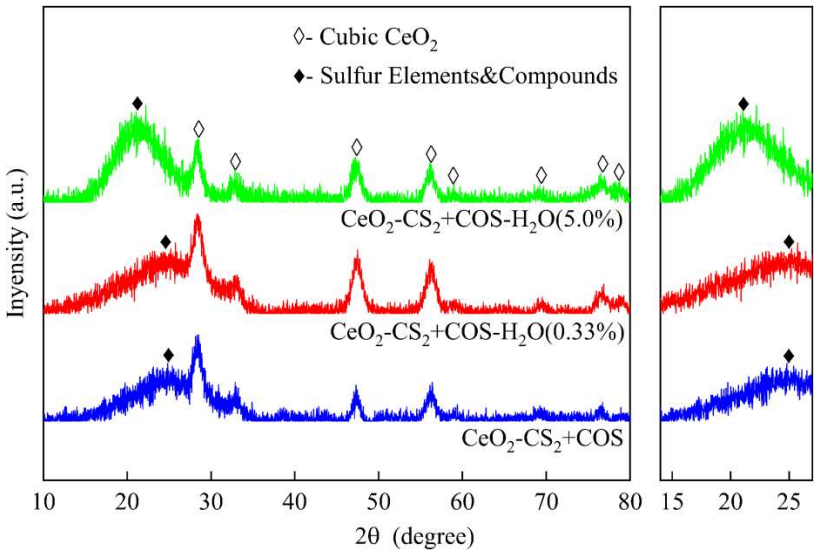

Fig. 5. The XRD patterns (Left) and the locally enlarged XRD (14~27 °) (Right) of as-prepared sulfated catalysts.

Fig. 6 gives the Raman spectra of CeO_2, CeO_2-CS_2+COS, CeO_2-CS_2+COS-H_2O(0.33%) and CeO_2-CS_2+COS-H_2O(5.0%) catalysts, and it can be found that three peaks are detected at 464 cm^{-1}, 600 cm^{-1} and 1180 cm^{-1} for pure CeO_2 catalyst, respectively. The first prominent peak is related to the symmetric stretching vibration of Ce-O-Ce, which is assigned to the F_{2g} characteristic vibration of cubic fluorite CeO_2, while the last two vibration peaks are attributed to

the surface oxygen defects [56,57]. It is evident that the low-temperature gas-phase sulfation of CS_2+COS makes the F_{2g} characteristic peak of CeO_2 shift to a lower wave number via altering its Ce-O-Ce structure [58-60], and the introduction of H_2O further improves the FWHM (full width at half-maximum) and peak intensity of F_{2g} vibration peak significantly. This indicates that the introduction of H_2O strengthens the influence of CS_2+COS low-temperature gas-phase sulfation on refining the grain size of nanoparticles on CeO_2 surface, which is in accordance with the results of SEM and XRD. Jang et al. [61] found that the introduction of SiO_2 refined the particle size of CeO_2 with a wider FWHM of the F_{2g} vibration peak detected for the core/shell CeO_2-SiO_2. Furthermore, the relative concentration of oxygen vacancies on the catalyst surfaces could be obtained by calculating the integral area ratio of the peaks at 600 cm^{-1}+1180 cm^{-1} and the peak of F_{2g} characteristic vibration [62]. As shown in Fig. S4, the introduction of H_2O improves the promotional effect of organic CS_2+COS low-temperature gas-phase sulfation on the relative concentration of oxygen vacancies on CeO_2 surface, but high concentration H_2O decreases this promotional effect. And the calculated relative concentrations of oxygen vacancies are as follow: CeO_2-CS_2+COS-H_2O(0.33%) > CeO_2-CS_2+COS-H_2O(5.0%) > CeO_2-CS_2+COS > CeO_2, which is consistent with the NH_3-SCR activity of catalysts. Therefore, the introduction of H_2O further helps to the generation of oxygen vacancies during the gas-phase sulfation process of organic CS_2+COS at 50 ºC, thus accelerating the conversion frequency between the chemisorbed oxygen and lattice oxygen via the Ce^{3+}/Ce^{4+} ion pair, which might be beneficial to promote the oxidation of NO to NO_2 and improves the NO_x conversion through the 'fast SCR' reaction [63-65].

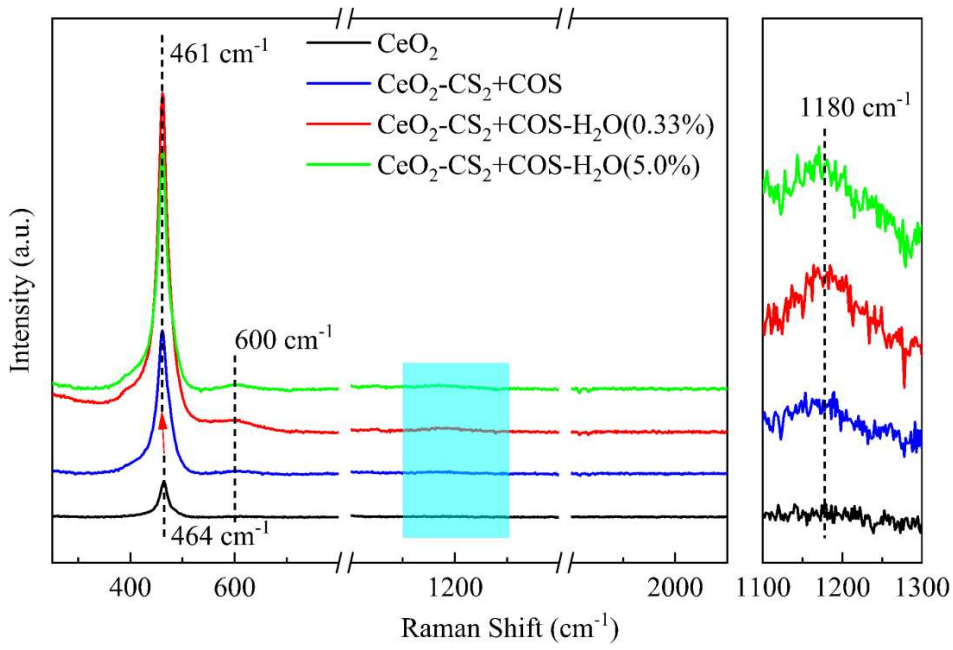

Fig. 6. Raman spectra of the as-prepared CeO_2 catalysts.

The FTIR spectra of CeO_2-CS_2+COS, CeO_2-CS_2+COS-H_2O(0.33%), and CeO_2-CS_2+COS-H_2O(5.0%) catalysts are given in Fig. 7. The vibration peaks located at 1627 cm^{-1} and 3417 cm^{-1} are attributed to the bending vibration and stretching vibration of -OH group, respectively [66]. When the content H_2O increases to 5.0% during the low-temperature gas-phase sulfation process, a new weak vibration peak attributed to H_2O appears at 847 cm^{-1} in CeO_2-CS_2+COS-H_2O(5.0%) [67]. Meanwhile, the formation of sulfate species during the low-temperature gas-phase sulfation results in the detection of multiple vibrational bands at 900~1300 cm^{-1}. Among them, the vibration peaks at 979 cm^{-1} and 1043 cm^{-1} are attributed to the characteristics of inorganic chelated bidentate sulfates, caused by the S-O and S=O bond vibrations of surface sulfate species, while the bands at 1116 and 1190 cm^{-1} are caused by the formed bulk sulfates on catalysts surface [65,68]. However, the enhancement of H_2O content from 0.33 vol.% to 5.0 vol.% weakens the intensity of the vibrational band caused by sulfate species, which is reasonable due to the enhanced interaction between the groups of -OH and SO_4^{2-} [69].

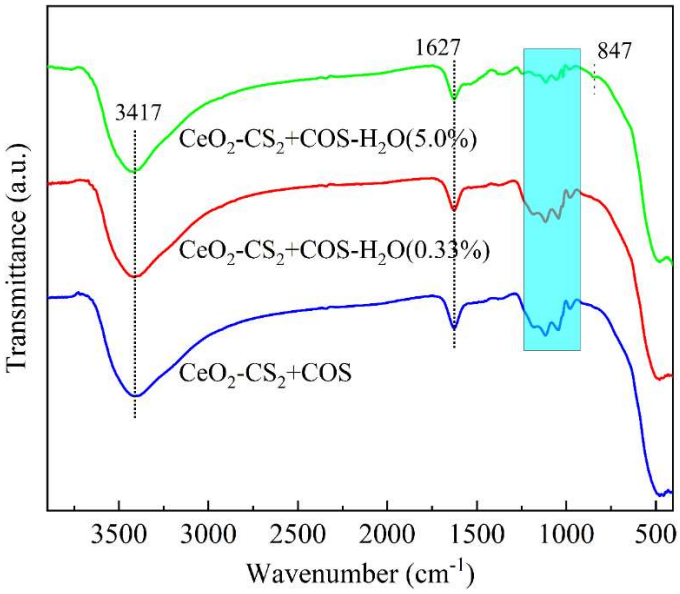

Fig. 7. FTIR spectra of the sulfated CeO_2 catalysts by $COS+CS_2$ at 50 °C.

3.4. Surface active components analysis

In this section, XPS (X-ray Photoelectron Spectroscopy) technique was employed to investigate the influence of H_2O introduction on the dispersion of elements on catalysts surface. As shown in Fig. 8(A), the Ce 3d XPS spectra could be deconvoluted into eight peaks via the Lorentz/Gaussian method. Among them, u' and v' are attributed to Ce^{3+} species ($3d^{10}$ $4f^{1}$), and the other peaks are ascribed to the Ce^{4+} electronic state ($3d^{10}$ $4f^{0}$) [49]. In addition, the low-temperature gas-phase sulfation of organic CS_2+COS increases the molar ratio of $Ce^{3+}/(Ce^{3+}+Ce^{4+})$ on CeO_2 surface and makes the Ce 3d spectra of catalyst shift to a higher binding energy direction by approximately 0.6 eV, indicating the electron-induced effect between Ce, O and S species, which alters the electron cloud density around Ce [70,71]. Interestingly, the introduction of H_2O improves this electron-induced effect and further increases the molar ratio of $Ce^{3+}/(Ce^{3+}+Ce^{4+})$ on CeO_2-CS_2+COS surface. However, as shown in Table 2, the enhancement of H_2O concentration from 0.33 vol.% to 5.0 vol.% reduces this promotional effect and makes the surface $Ce^{3+}/(Ce^{3+}+Ce^{4+})$ molar ratio of CeO_2-CS_2+COS-H_2O(0.33%) decrease from 36.42 % to 33.15%. Generally, the generation of oxygen vacancies is associated with the electron transfer of Ce^{4+}/Ce^{3+} ion pair, and the presence of Ce^{3+} can aggravate the charge imbalance and promote the redox cycle of Ce^{4+}/Ce^{3+}, thus heightens the activation of oxygen on the catalysts surfaces and results in the generation of more oxygen vacancies [72,73]. Therefore, the further enhancement of H_2O introduction on the surface $Ce^{3+}/(Ce^{3+}+Ce^{4+})$ molar ratio of

CeO_2-CS_2+COS might be an important reason for increasing the NH_3-SCR activity of catalyst. However, the introduction of higher concentration H_2O (5.0 vol.%) results in a stronger competitive adsorption between H_2O and organic CS_2+COS, which might affect the conversion of the adsorbed CS_2+COS on cubic fluorite CeO_2 surface, thus decreases the $Ce^{3+}/(Ce^{3+}+Ce^{4+})$ molar ratio of CeO_2-CS_2+COS-H_2O(0.33%).

As shown in Fig. 8(B), the O 1s spectrum of pure CeO_2 can be fitted into three peaks, which belongs to the lattice oxygen existing in cubic fluorite CeO_2 (O_α, 529.1 eV), the chemisorbed oxygen (O_β, 530.0 eV) and the lattice oxygen bonded with Ce_2O_3 (O_γ, 531.8 eV), respectively [74]. Meanwhile, the low-temperature gas-phase sulfation of CS_2+COS leads the O 1s XPS binding energy of CeO_2 shifting to a higher value, while only O_α and O_β are detected for the sulfated CeO_2 catalysts due to the formation of Ce-O-S bonds [75]. Interestingly, the introduction of H_2O further increases the binding energy of O 1s of CeO_2-CS_2+COS catalyst. Furthermore, as shown in Table 2, the presence of H_2O during the low-temperature gas-phase sulfation of CS_2+COS improves the concentration of chemical adsorption oxygen (O_β) on catalyst surface, but excessive water leads to a decrease of this value. The regular pattern of H_2O introduction on the surface O_β concentration is in accordance with that of $Ce^{3+}/(Ce^{3+}+Ce^{4+})$ molar ratio. A large number of studies had demonstrated that the surface chemisorbed oxygen had a higher mobility than the lattice oxygen, which was easy to be activated and played an important role in the oxidation reaction. Consequently, higher surface molar ratio of $O_\beta/(O_\alpha+O_\beta+O_\gamma)$ are generally regarded to be beneficial to improve the oxidization of NO to NO_2 and the 'fast SCR' process ($NO + NO_2 + 2NH_3 = 2N_2 + 3H_2O$) [76,77].

From Fig. 8(C), it can be found that the S 2p spectra of the sulfated CeO_2 catalysts can be fitted into three peaks located at 163.8 eV, 168.3 eV and 169.3 eV (±0.3 eV), and the last two peaks belong to S^{6+} species. Meanwhile, the peak located about 163.8 eV is attributed to sulfur, which is different from the formation of sulfate species (SO_4^{2-}, etc.) in CeO_2 catalyst during the gas-phase sulfation of inorganic SO_2 [54,78]. However, the introduction of H_2O decreases the intensity of S 2p spectra of CeO_2-CS_2+COS, thereby reduces the concentrations of the formed S^{6+} and S species on catalyst surface. As shown in Table 2, the introduction of H_2O during the low-temperature gas-phase sulfation of CS_2+COS helps to increase the surface molar ratio $S^{6+}/(S^{6+}+S)$, and the enhancement of H_2O concentration from 0.33 vol.% to 5.0 vol.% not only

increases the formed surface total concentration of S^{6+} and S, but also further improves the molar ratio $S^{6+}/(S^{6+}+S)$ on CeO_2-CS_2+COS-H_2O(0.33%) surface. Therefore, it can be included that lower concentration of sulfur-containing species might be helpful to the NH_3-SCR activity of the sulfated CeO_2 catalyst.

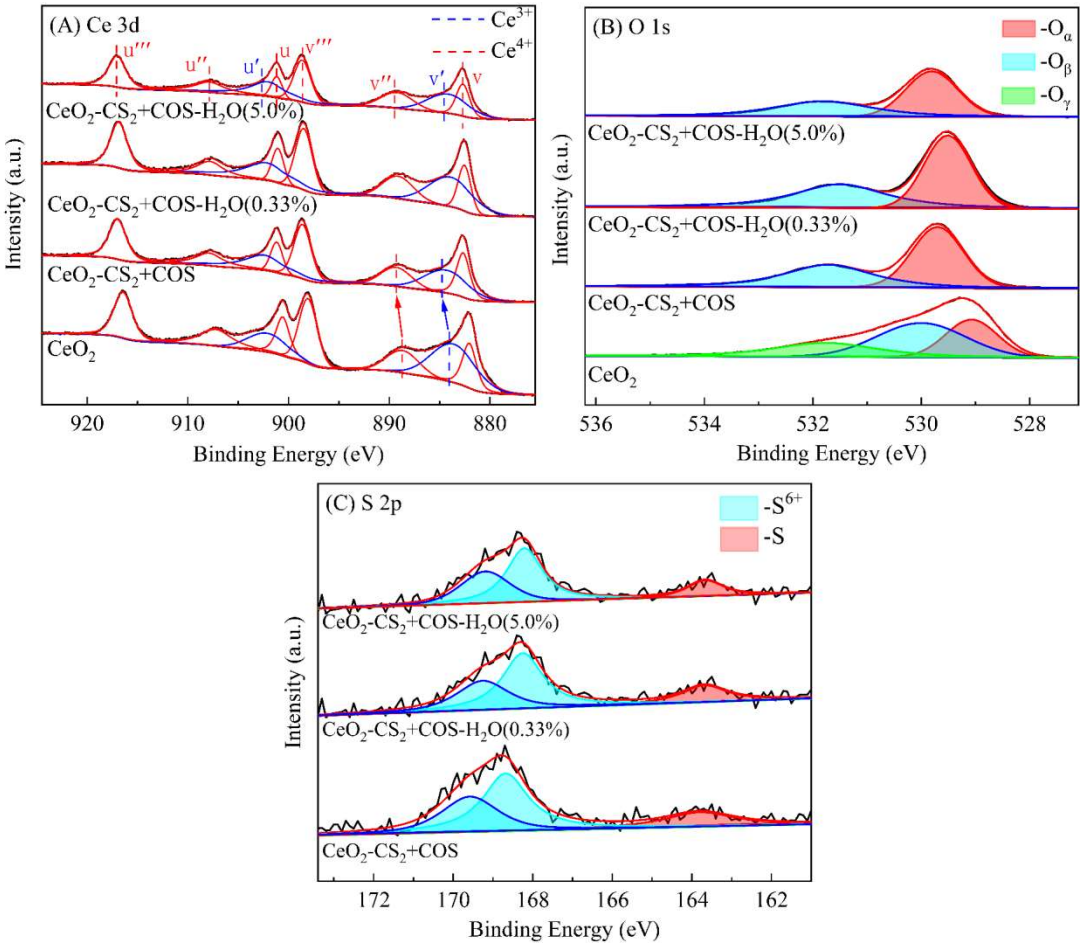

Fig. 8. (A) Ce 3d, (B) O 1s, and (C) S 2p XPS spectra of the as-prepared catalyst.

Table 2 Surface composition and atomic ratio of the as-prepared catalysts calculated from XPS

Catalysts	Atomic concentrations (%)			Atomic ratios (%)		
	Ce	O	S*	$Ce^{3+}/(Ce^{3+}+Ce^{4+})$	$O_\beta/(O_\alpha+O_\beta+O_\gamma)$	$S^{6+}/(S^{6+}+S)$
CeO_2	36.16	63.84	-	31.34	44.16	-
CeO_2-CS_2+COS	32.15	63.24	4.61	31.75	44.69	80.60
CeO_2-CS_2+COS-H_2O(0.33%)	32.73	63.94	3.33	36.42	46.79	82.20
CeO_2-CS_2+COS-H_2O(5.0%)	33.25	62.73	4.02	33.15	45.19	85.98

* The sum of S and S^{6+}.

3.5. Thermogravimetric analysis

Thermogravimetric analysis was done to further investigate the influence of H_2O introduction on the formed sulfur-containing species over CeO_2-CS_2+COS-H_2O catalyst. The results are shown in Fig. 9. It can be clearly seen that there exists an apparent weight-loss for the TG-DTG curves as the temperature increases, which can be divided into three parts. The weight loss peak observed in the range of 30-200 °C is attributed to the desorption of physically absorbed water and dehydroxylation [52,72], and the desorbed values in this stage are 2.14%, 2.44% and 2.37% for CeO_2-CS_2+COS, CeO_2-CS_2+COS-H_2O(0.33%) and CeO_2-CS_2+COS-H_2O(5.0%), respectively. Consequently, the introduction of H_2O slightly increases the content of physically adsorbed water and hydroxyl groups in the sulfated CeO_2 catalysts by organic CS_2+COS at 50 °C, which might be beneficial to the NH_3-SCR activity of catalyst. Guo et al. [79] claimed that SO_4^{2-}, O_2^{2-} and hydroxyl-like (-OH) species could function as Brønsted acid sites to enhance the adsorption of NH_3 and consequently improved the NO_x removal efficiency of catalyst. Peng et al. [80] also mentioned that sulfate species promoted the ionization of water adsorbed on the catalyst surfaces, resulting in the formation of more hydroxyl group and more Brønsted acid sites. In addition, the XRD and XPS analyses validate the formation of sulfur element in the sulfated CeO_2-CS_2+COS, CeO_2-CS_2+COS-H_2O(0.33%) and CeO_2-CS_2+COS-H_2O(5.0%) catalysts. Thus, the slight weight losses observed between 200-600 °C might be ascribed to the emission of SO_2 due to the oxidation reaction of sulfur and oxygen-containing functional groups in this temperature range. Finally, the third stage of weight losses began at 650 °C is attributed to the thermal decomposition of sulfate species [37,38], and approximately 5.44 %, 4.07 % and 3.07 % were calculated for CeO_2-CS_2+COS, CeO_2-CS_2+COS-H_2O(0.33%) and CeO_2-CS_2+COS-H_2O(5.0%) catalysts, respectively. Therefore, the introduction of H_2O decreases the formed amount of sulfate species in the sulfated CeO_2 catalysts, although they had been reported to adsorb NH_3 as a stable acidic site and presented a strong thermal stability. And it can be inferred that there exists a competitive adsorption of H_2O and CS_2+COS on cubic fluorite CeO_2 surface, which reduces the formation of sulfate species, but the hydroxyl groups dissociated by H_2O enhances the interaction between organic CS_2+COS and cubic fluorite CeO_2, which affects the physical and chemical properties of catalyst. Furthermore, the appropriate amount of -OH group as the additives for Brønsted acid sites enhances the

adsorption capacity of NH_3 [46]. However, excess water significantly inhibits the chemical adsorption of CS_2 and COS on catalyst surfaces due to a stronger competitive adsorption among them and depresses the hydrolysis of organic sulfur, thus further reduces the production of sulfate species in CeO_2 catalyst. This demonstrates that the positive impact of hydroxyl groups might be outweighed by the negative effect of the competitive adsorption of H_2O and COS/CS_2 under the condition of excess water [26,81], although the enhancement of H_2O concentration from 0.33 vol.% to 5.0 vol.% further improves the molar ratio of $S^{6+}/(S^{6+}+S)$ on CeO_2 surface calculated from the results of XPS spectra.

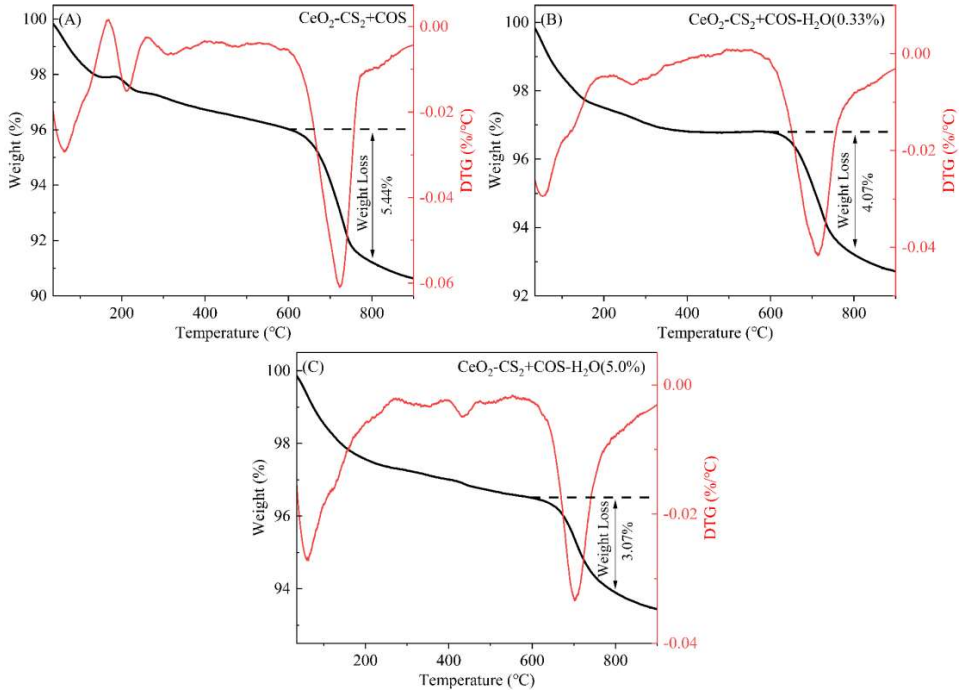

Fig. 9. The TG-DTG curves of CeO_2-CS_2+COS, CeO_2-CS_2+COS-H_2O(0.33%) and CeO_2-CS_2+COS-H_2O(5.0%) catalysts.

3.6. The properties of redox ability

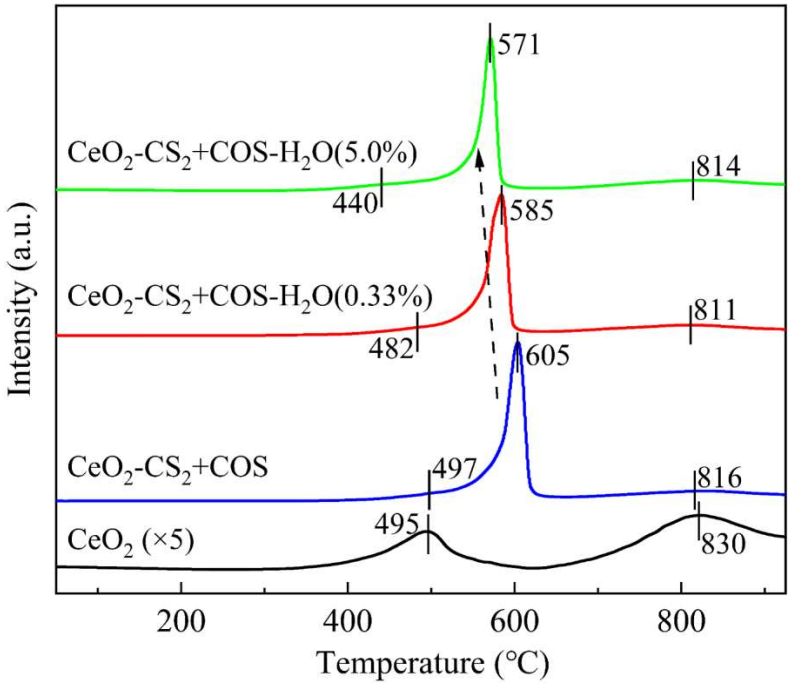

Fig. 10. The H_2-TPR patterns of CeO_2, CeO_2-CS_2+COS, CeO_2-CS_2+COS-H_2O(0.33%) and CeO_2-CS_2+COS-H_2O(5.0%) catalysts.

H_2-TPR was carried out to investigate the influence of H_2O introduction on the reducibility of CeO_2-CS_2+COS catalyst and the results are shown in Fig. 10. It is reported that two reduction peaks of pure CeO_2 at about 495 °C and 830 °C belongs to the reduction of surface Ce^{4+} to Ce^{3+} and bulk Ce^{4+} to Ce^{3+} [61], respectively. Meanwhile, the low-temperature gas-phase sulfation of CS_2+COS makes the reduction peak of CeO_2 at 495 °C shifting to left and disappearing due to the formation of surface sulfate and the interaction of Ce and S species in the catalyst [70,82]. Furthermore, this treatment also leads the reduction peak of bulk CeO_2 at 830 °C shifting to a lower temperature owing to the enhanced mobility of the lattice oxygen for cubic fluorite CeO_2 by the gas-phase sulfation of reductive organic CS_2+COS [83], thus improves the reducibility of bulk CeO_2. It should be mentioned that a new high peak attributed to the reduction of surface sulfate species appears at 605 °C, 585 °C and 571 °C for the sulfated CeO_2-CS_2+COS, CeO_2-CS_2+COS-H_2O(0.33%) and CeO_2-CS_2+COS-H_2O(5.0%) catalysts, respectively [34]. According to previous studies, the formation of sulfate species increased the surface active oxygen concentration, thus enhanced the adsorption of NH_3 and promoted the low-temperature oxidation of NO [40,65]. This indicates that the gas-phase sulfation of organic CS_2+COS increases the reducibility of CeO_2 catalyst effectively. Furthermore, the introduction of H_2O

makes the reduction peak ascribed to sulfate species of CeO_2-CS_2+COS moving to the low temperature direction, which implies that the gas-phase sulfation of organic CS_2+COS at the presence of water helps to further improve the reducibility of sulfate species although their formed amounts also decrease. Therefore, the introduction of H_2O further contributes to improve the reducibility of CeO_2-CS_2+COS, which is beneficial to the NH_3-SCR activity of the catalyst.

3.7. The properties of surface acidity

Similar to the redox ability, the surface acidity is regarded as another critical factor of influencing the NH_3-SCR activity of catalyst. Therefore, the NH_3-TPD test was carried out to investigate the effect of H_2O introduction on the surface acidity of CeO_2-CS_2+COS during the low-temperature gas-phase of organic CS_2+COS. According to the NH_3-TPD spectrum in Fig. 11, a wide desorption peak of NH_3 species was observed at 50-450 °C, which was attributed to weak acid sites and medium-strong acid sites via fitting it into five desorption peaks (labeled as I, II, III, IV and V) [84]. Previous studies indicate that there exists a positive correlation between the surface acid sites and the desorption temperature of NH_3 species for the NH_3-SCR catalysts [85,86]. Therefore, the relative ratio of the integrated area for these five NH_3 desorption peaks were calculated, as summarized in Table 3. Pure CeO_2 has a considerable proportion of weak acid sites (74.83 %), but the low-temperature gas-phase sulfation of CS_2+COS significantly increases the proportion of medium-strong acid sites, which is further enhanced by introducing H_2O during the sulfation process, although the introduction of H_2O decreases the formed amount of surface or/and bulk sulfation species according to the results of XPS spectra and TG-DTG curves. Jin et al. [87] pointed out that the inclusion of HSiW resulted in an increase of the surface acid sites of CeO_2, especially the number of medium-strong acid sites, thus improved the NH_3-SCR activity of catalyst. This phenomenon was also reported in the Cu-SSZ-13 catalyst [88]. Therefore, the intensity of medium-strong acid sites plays a significant impact on the NH_3-SCR activity, and the formation of sulfate species helps to enhance the intensity of medium-strong acid sites for CeO_2 catalyst, which has also been proven by the gas-phase sulfation of CS_2+COS at 50 °C. Furthermore, the introduction of 0.33 vol.% H_2O makes the CeO_2-CS_2+COS-H_2O(0.33%) catalyst presenting the best medium-strong acid intensity, although it decreases the formed amount of surface or/and bulk sulfation species. The increase of H_2O content from 0.33 vol.% to 5.0 vol.% increases the amount of sulfate species detected on

CeO_2-CS_2+COS-H_2O(0.33%) surface according to XPS results, but slightly reduces its medium-strong acid sites. This may be one of the reasons for the decrease of the catalytic performance of CeO_2-CS_2+COS-H_2O(0.33%), and thus both the surface sulfate species and the bulk sulfate species can affect the NH_3-SCR acidity of CeO_2 catalyst.

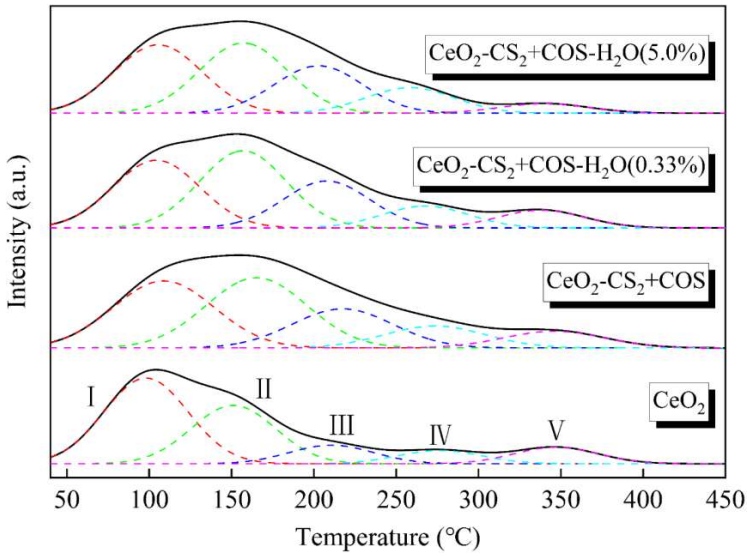

Fig. 11. The fitted NH_3-TPD curves of CeO_2, CeO_2-CS_2+COS, CeO_2-CS_2+COS-H_2O(0.33%) and CeO_2-CS_2+COS-H_2O(5.0%) catalysts.

Table 3 The surface acidities of the as-prepared catalysts

Samples	Relative ratio of desorption sub-peaks (%)					Relative ratio of different acids (%)	
	Peak I	Peak II	Peak III	Peak IV	Peak V	Weak acid	Medium-strong acid
CeO_2	44.49	30.34	9.67	6.89	8.61	74.83	25.17
CeO_2-CS_2+COS	31.18	32.65	18.18	10.22	7.77	63.83	36.17
CeO_2-CS_2+COS-H_2O(0.33%)	29.25	33.32	20.27	9.48	7.68	62.57	37.43
CeO_2-CS_2+COS-H_2O(5.0%)	30.90	31.76	21.43	11.56	4.35	62.66	37.34

As an essential reactant for the hydrolysis of organic CS_2 or/and COS, the introduction of appropriate H_2O could enhance the adsorption and conversion performance of organic sulfur on the surface of metal oxide catalysts [89,90]. Therefore, water was introduced into the low-temperature gas-phase sulfation of CS_2+COS over CeO_2 catalyst in order to further improve its NH_3-SCR activity for the first time, and the introduction of 0.33 vol.% H_2O promotes the adsorption of CS_2+COS on cubic fluorite CeO_2 surface and the interaction among them, thus

further enhances the optimization effect of reducing organic CS_2+COS on the electronic state of CeO_2. This increases the content of Ce^{3+} ions, chemisorbed oxygen (O_β) and oxygen vacancies on CeO_2-CS_2+COS surface. Furthermore, the introduction of appropriate amount of H_2O effectively enhances the redox cycle of Ce^{4+}/Ce^{3+} ion pairs, and further increases the medium-strong acid although it decreases the formed amount of surface or/and bulk sulfation species for the sulfated CeO_2 catalyst by organic CS_2+COS at 50 °C. These all help to improve the NH_3-SCR performance of CeO_2 catalyst. However, excess water (5.0 vol.%) enhances the competitive adsorption of H_2O and COS/CS_2, which is slightly unbeneficial to the promotional effect of water introduction on the NH_3-SCR activity of CeO_2 catalyst during the gas-phase sulfation of CS_2+COS at 50 °C.

4. Conclusions

In summary, as an indispensable key reactant for the hydrolysis reaction of organic sulfur, H_2O was introduced during the low-temperature gas-phase sulfation of CS_2+COS, which has been verified to be a simple and effective method to improve the NH_3-SCR performance of CeO_2 catalyst. The formation of hydroxyl groups dissociated from H_2O are beneficial to the adsorption of CS_2 and COS on CeO_2 surface, and enhances the interaction among them, although the introduction of H_2O decreases the formed amount of surface or/and bulk sulfation species. Furthermore, the introduction of H_2O increases the concentrations of Ce^{3+} ions, chemisorbed oxygen (O_β) and oxygen vacancies on CeO_2-CS_2+COS surface, which also effectively enhances the redox cycle of Ce^{4+}/Ce^{3+} ion pairs and increases the medium-strong acid sites. These all contributes to further improving the promotional effect of CS_2+COS low-temperature gas-phase sulfation on the NH_3-SCR activity of CeO_2. However, it is imperative to be noted that the introduction of excessive H_2O might result in a reduced diffusion of COS and CS_2 on the hydrolysis center of CeO_2 and weakens their interaction during the low-temperature gas-phase sulfation, negating the promotional effect of H_2O introduction on the NH_3-SCR activity of the CeO_2-CS_2+COS catalyst. The study can provide a scientific reference for the development of the CeO_2-based catalysts in the practical application of NH_3-SCR technology.

CRediT authorship contribution statement

Jiaxing Liu: Writing - original draft, Methodology, Validation. **Zhenchang Sun and Yafei Zhu:** Software

and Methodology. **Yanping Du:** Writing - review & editing. **Zhibo Xiong:** Conceptualization, Funding acquisition, Writing - review & editing. **Fei Zhou:** Investigation, Supervision. **Jing Jin:** Investigation, Supervision, Funding acquisition. **Qiguo Yang:** Investigation, Supervision, Writing - review & editing. **Wei Lu:** Investigation, Supervision, Funding acquisition.

Declaration of Competing Interest

The authors declare that they have no known competing financial interests or personal relationships that could have appeared to influence the work reported in this paper.

Acknowledgements

This work was supported by the National Science Foundation of China (No. 51406118), the Bureau of Shanghai Municipal Science and Technology (No. 23010503500), Program of Special Appointment (Eastern Scholar) at Shanghai Institutions of Higher Learning (No. QD2015017).

References

[1] A.T. Anastasopolos, U.M. Sofowote, P.K. Hopke, M. Rouleau, T. Shin, A. Dheri, H. Peng, R. Kulka, M. D Gibson, P. Farah, N. Sundar. Air quality in Canadian port cities after regulation of low-sulphur marine fuel in the North American Emissions Control Area. Sci. Total. Environ. 791 (2021) 147949, https://doi.org/10.1016/j.scitotenv.2021.147949.

[2] Q. Lyu, Y. Guan, Y.H. Liu. Research progress on Hg removal performance of Ce-containing materials. Clean. Coal. Technol. 28 (2022) 69-83, https://doi.org/10.13226/j.issn.1006-6772.LH22062501.

[3] H. Caglayan, H. Caliskan. Thermo-ecological analysis of industrial kilns. J. Environ. Manage. 241 (2019) 149-155, https://doi.org/10.1016/j.jenvman.2019.04.032.

[4] M. Heidari, M. Tahmasebpoor, S.B. Mousavi, C. Pevida. CO_2 capture activity of a novel CaO adsorbent stabilized with (ZrO_2+Al_2O_3+CeO_2)-based additive under mild and realistic calcium looping conditions. J. CO_2. Util. 53 (2021) 101747, https://doi.org/10.1016/j.jcou.2021.101747.

[5] S.B. Mousavi, M. Heidari, F. Rahmani, R.A. Sene, P.T. Clough, S. Ozmen. Highly robust ZrO_2-stabilized

CaO nanoadsorbent prepared via a facile one-pot MWCNT-template method for CO_2 capture under realistic calcium looping conditions. J. Clean. Prod. 384 (2023) 135579, https://doi.org/10.1016/j.jclepro.2022.135579.

[6] R.L. Shao, S.W. Han, C.B. Xuan, L.Y. Wang, X.Y. Zhang, X.X. Cheng, Z.Q. Wang. Influence mechanism of Na-K synergism on the evolution of NO_x in wet NO reduction. Clean. Coal. Technol. 29 (2023) 166-175, https://doi.org/10.13226/j.issn.1006-6772.23051201.

[7] J.N. Liu, X. Wu, B.H. Hou, Y.L. Du, L.L. Liu, B.S. Yang. $NiMn_2O_4$ sphere catalyst for the selective catalytic reduction of NO by NH_3: Insight into the enhanced activity via solvothermal method, J. Environ. Chem. Eng. 9 (2021) 105152, https://doi.org/10.1016/j.jece.2021.105152.

[8] Y.Y. Tan, X.R. Zheng, G.Y. Tian, Y.J. Li. Mechanism of SO_2 removal by Mn-Ce high-content iron ash. Clean. Coal. Technol. 29 (2023) 89-97, https://doi.org/10.13226/j.issn.1006-6772.21111703.

[9] R.X. Xiao, K.F. Chao, J. Liu, M.H. Chen, X.B. Zhu, B. Fu. Screening of Absorbents for Viscose Fiber CS_2 Waste Air and Absorption-Desorption Process. Atmosphere. 14 (2023) 602, https://doi.org/10.3390/atmos14030602.

[10] X.Y. Xu, Y.L. Wang, P.F. Chen, T.Y. Zhao, Z.R. Gong, B.X. Wang, S.B. Huang. Removal of NO_x from flue gas using different agricultural wastes as carbon sources: Performance and microbial communities. J. Environ. Chem. Eng. 11 (2023) 109804, https://doi.org/10.1016/j.jece.2023.109804.

[11] C.S. Yoo, S. Duwal, M. Kim, Y. Ohishi. Phase diagram of carbonyl sulfide: An analogy to carbon dioxide and carbon disulfide. Jap. J. Appl. Phys. 56 (2017) 05FA04, https://doi.org/10.7567/JJAP.56.05FA04.

[12] R. Cao, X.Q. Wang, P. Ning, Y.B. Xie, L.L. Wang, Y.X. Ma, X. Li, H. Zhang, J.Y. Liu. Advantageous Role of N-doping on K@Al in COS/CS_2 Hydrolysis: Diminished Oxygen Mobility and Rich basic sites. Fuel. 337 (2023) 126882, https://doi.org/10.1016/j.fuel.2022.126882.

[13] X. Kan, G.Q. Zhang, Y.Y. Luo, F.J. Liu, Y. Zheng, Y.H. Xiao, Y.N. Cao, C.T. Au, S.J. Liang, L.L. Jiang. Efficient catalytic removal of COS and H_2S over graphitized 2D micro-meso-macroporous carbons endowed with ample nitrogen sites synthesized via mechanochemical carbonization. Green. Energy. Environ. 7 (2022) 983-995, https://doi.org/10.1016/j.gee.2020.12.016.

[14] S.J. Liang, J.X. Mi, F.J. Liu, Y. Zheng, Y.H. Xiao, Y.N. Cao, L.L. Jiang. Efficient catalytic elimination of COS and H_2S by developing ordered mesoporous carbons with versatile base N sites via a calcination induced self-assembly rout. Chem. Eng. Sci. 221 (2020) 115714, https://doi.org/10.1016/j.ces.2020.115714.

[15] J.L. Liang, M.W. Fan, M.M. Wu, J.W. Hua, W.S. Cai, T.T. Huang, Y.Q. Liu, C.G. Liu. In situ synthesis of MoS_2 nanoflakes within a 3D mesoporous carbon framework for hydrodesulfurization. J. Catal. 415 (2022) 153-164, https://doi.org/10.1016/j.jcat.2022.10.006.

[16] Y.R. Xu, P.Y. Li, S.H. Yuan, B.K. Sui, W.K. Lai, X.D. Yi, W.P. Fang. Sacrificial carbonaceous coating over alumina supported Ni-MoS_2 catalyst for hydrodesulfurization. RSC. Adv. 9 (2019) 11951, https://doi.org/10.1039/C9RA00884E.

[17] L.L. Mguni, Y.L. Yao, X.Y. Liu, Z.Y. Yuan, D. Hildebrandt. Ultra-deep desulphurization of both model and commercial diesel fuels by adsorption method. J. Environ. Chem. Eng. 7 (2019) 102957, https://doi.org/10.1016/j.jece.2019.102957.

[18] R. Saeedirad, A. Rashidi, M. Daraee, M. Bazmi, S. Askari. Synthesis of Nitrogen-Doped CNT-Based MOF Hybrids for Adsorptive Desulfurization of the Gas Stream. ChemistrySelect. 5 (2020) 13530-13536, https://doi.org/10.1002/slct.202002618.

[19] P. Xu, Z.H. Jin, T.Y. Zhang, X.F. Chen, M.H. Qiu, Y.Q. Fan. Fabrication of a Ceramic Membrane with Antifouling PTFE Coating for Gas-Absorption Desulfurization. Ind. Eng. Chem. Res. 60 (2021) 2492-2500,

https://doi.org/10.1021/acs.iecr.1c00338.

[20] H.Y. Wang, H.H. Yi, P. Ning, X.L. Tang, L.L. Yu, D. He, S.Z. Zhao. Calcined hydrotalcite-like compounds as catalysts for hydrolysis carbonyl sulfide at low temperature. Chem. Eng. J. 166 (2011) 99-104, https://doi.org/10.1016/j.cej.2010.10.025.

[21] H.Y. Wang, H.H. Yi, X.L. Tang, P. Ning, L.L. Yu, D. He, S.Z. Zhao, K. Li. Catalytic hydrolysis of COS over calcined CoNiAl hydrotalcite-like compounds modified by cerium. Appl. Clay. Sci. 70 (2012) 8-13, http://dx.doi.org/10.1016/j.clay.2012.09.008.

[22] E.Y. He, G. Huang, H.L. Fan, C. Yang, H. Wang, Z. Tian, L.J. Wang, Y.R. Zhao. Macroporous alumina- and titania-based catalyst for carbonyl sulfide hydrolysis at ambient temperature. Fuel. 246 (2019) 277-284, https://doi.org/10.1016/j.fuel.2019.02.097.

[23] J.X. Qu, X.Q. Wang, L.L. Wang, B.W. Xu, P. Ning, Y.X. Ma, Y.B. Xie, R. Cao, Q. Ma. The investigation of the role of nitrogen in the improvement of catalytic activity and stability of Zr/Ti-based material for carbon disulfide hydrolysis. Sep. Purif. Technol. 269 (2022) 121357, https://doi.org/10.1016/j.seppur.2022.121357.

[24] Y.F. Wang, L. Ding, H.M. Long, J.J. Xiao, L.X. Qian, H.T. Wang, C.B. Xu. Carbonyl sulfur removal from blast furnace gas: Recent progress, application status and future development. Chemosphere 307 (2022) 136090, https://doi.org/10.1016/j.chemosphere.2022.136090.

[25] J.N. Gu, J.X. Liang, S.J. Hu, Y.X. Xue, X. Min, M.M. Guo, X.F. Hu, J.P. Jia, T.H. Sun. Enhanced removal of COS from blast furnace gas via catalytic hydrolysis over Al_2O_3-based catalysts: Insight into the role of alkali metal hydroxide. Sep. Purif. Technol. 295 (2022) 121356, https://doi.org/10.1016/j.seppur.2022.121356.

[26] X. Sun, H.T. Ruan, X. Song, L.N. Sun, K. Li, P. Ning, C. Wang. Research into the reaction process and the

effect of reaction conditions on the simultaneous removal of H_2S, COS and CS_2 at low temperature. RSC. Adv. 8 (2018) 6996, https://doi.org/10.1039/C7RA12086A.

[27] Y.L. Liu, P. Wu, K. Shen, Y.P. Zhang, G.B. Li, B. Li. Contribution of Na/K Doping to the Activity and Mechanism of Low-Temperature COS Hydrolysis over TiO_2‑Al_2O_3 Based Catalyst in Blast Furnace Gas. ACS. Omega. 7 (2022) 13299-13312, https://doi.org/10.1021/acsomega.2c00968.

[28] P.T. Gao, Y.R. Li, Y.T. Lin, L.P. Chang, T.Y. Zhu. Promoting effect of Fe/La loading on γ-Al_2O_3 catalyst for hydrolysis of carbonyl sulfur. Environ. Sci. Pollut. R. 29 (2022) 84166-84179, https://doi.org/10.1007/s11356-022-20928-1.

[29] L. Wang, S.D. Wang, Q. Yuan, G.Z. Lu. COS hydrolysis in the presence of oxygen: Experiment and modeling. J. Nat. Gas. Chem. 17 (2008) 93-97, https://doi.org/10.1016/S1003-9953(08)60032-8.

[30] R.H. Sui, C.B. Lavery, C.E. Deering, R. Prinsloo, D. Li, N. Chou, K.L. Lesage, R.A. Marriott. Improved carbon disulfide conversion: Modification of an alumina Claus catalyst by deposition of transition metal oxides. Appl. Catal. A 604 (2020) 117773, https://doi.org/10.1016/j.apcata.2020.117773.

[31] S.Z. Zhao, H.H. Yi, X.L. Tang, D.J. Kang, F.Y. Gao, J.G. Wang, Y.H. Huang, Z.Y. Yang. Calcined ZnNiAl hydrotalcite-like compounds as bifunctional catalysts for carbonyl sulfide removal. Catal. Today. 327 (2019) 161-167, https://doi.org/10.1016/j.cattod.2018.05.011.

[32] C. Zhang, J.C. Li, D.L. Fang, P. Tan, L. Ma, Q.Y. Fang, G. Chen. Research progress on anti-poisoning of Mn-based low temperature SCR catalysts. Clean. Coal. Technol. 28 (2022) 110-135, https://doi.org/10.13226/j.issn.1006-6772.HK22072501.

[33] W. Wang, Z.B. Xiong, J. Jin, W. Lu, H.C. Shi. Influence of CS_2 pretreatment on the NH_3-SCR activity of CeO_2: Synergistic promotional effect of sulfation and reduction. J. Environ. Chem. Eng. 9 (2021) 106836, https://doi.org/10.1016/j.jece.2021.106836.

[34] J.J. Chen, W.T. Zhao, Q. Wu, J.X. Mi, X.Y. Wang, L. Ma, L.L. Jiang, C. Au, J.H. Li. Effects of anaerobic SO_2 treatment on nano-CeO_2 of different morphologies for selective catalytic reduction of NO_x with NH_3. Chem. Eng. J. 382 (2020) 122910, https://doi.org/10.1016/j.cej.2019.122910.

[35] W. Tan, J.M. Wang, S.H. Yu, A.N. Liu, L.L. Li, K. Guo, Y.D. Luo, S.H. Xie, F. Gao, F.D. Liu, L. Dong. Morphology-Sensitive Sulfation Effect on Ceria Catalysts for NH_3-SCR. Top. Catal. 63 (2020) 932-943, https://doi.org/10.1007/s11244-020-01342-8.

[36] S.J. Yang, Y.F. Guo, H.Z. Chang, L. Ma, Y. Peng, Z. Qu, N.Q. Yan, C.Z. Wang, J.H. Li. Novel effect of SO_2 on the SCR reaction over CeO_2: Mechanism and significance. Appl. Catal. B 136-137 (2013) 19-28, http://dx.doi.org/10.1016/j.apcatb.2013.01.028.

[37] L. Zhang, W.X. Zou, K.L. Ma, Y. Cao, Y. Xiong, S.G. Wu, C.J. Tang, F. Gao, L. Dong. Sulfated Temperature Effects on the Catalytic Activity of CeO_2 in NH_3-Selective Catalytic Reduction Conditions. J. Phys. Chem. C 119 (2015) 1155-1163, https://doi.org/10.1021/jp511282c.

[38] Q. Wu, X.P. Chen, J.X. Mi, S.X. Cai, L. Ma, W.T. Zhao, J.J. Chen, J.H. Li. The Absence of Oxygen in Sulfation Promotes the Performance of the Sulfated CeO_2 Catalyst for Low-Temperature Selective Catalytic Reduction of NO_x by NH_3: Redox Property versus Acidity. ACS. Sustain. Chem. Eng. 9 (2021) 967-979, https://doi.org/10.1021/acssuschemeng.0c08427.

[39] X.Y. Liu, P.L. Wang, Y.J. Shen, S.Y. Bi, W. Ren, D.S. Zhang. Boosting SO_2-Tolerant Catalytic Reduction of NO_x via Selective Adsorption and Activation of Reactants over Ce^{4+}-SO_4^{2-} Pair Sites. ACS. Catal. 12 (2022) 11306-11317, https://doi.org/10.1021/acscatal.2c02699.

[40] X.J. Yao, Z. Wang, S.H. Yu, F.M. Yang, L. Dong. Acid pretreatment effect on the physicochemical property and catalytic performance of CeO_2 for NH_3-SCR. Appl. Catal. A 542 (2017) 282-288, http://dx.doi.org/10.1016/j.apcata.2017.06.003.

[41] L. Ma, C.Y. Seo, M. Nahata, X.Y. Chen, J.H. Li, J.W. Schwank. Shape dependence and sulfate promotion of CeO_2 for selective catalytic reduction of NO_x with NH_3. Appl. Catal. B 232 (2018) 246-259, https://doi.org/10.1016/j.apcatb.2018.03.065.

[42] R.Y. Xie, L. Ma, K. Sun, G. Zhou, Z. Qu, N.Q. Yan. Catalytic performance and mechanistic evaluation of sulfated CeO_2 cubes for selective catalytic reduction of NO_x with ammonia. J. Hazard. Mater. 420 (2021) 126545, https://doi.org/10.1016/j.jhazmat.2021.126545.

[43] W. Wang, Z.B. Xiong, W.F. He, W. Lu, H.C. Shi. Influence of thiourea modification on the NH_3-SCR activity of CeO_2: Simultaneous tuning morphology and surface acidity. J. Energy. Inst. 98 (2021) 322-333, https://doi.org/10.1016/j.joei.2021.07.009.

[44] N.Y. Wang, X.Q. Wang, Y. Liu, Z.B. Wu. Storage-reduction strategy for NO_x reduction from gas turbine exhaust with W-Ti-CeO_x catalyst in natural gas power plants. J. Rare. Earths. 41 (2023) 933-940, https://doi.org/10.1016/j.jre.2022.11.011.

[45] X.J. Zhang, J.K. Wang, Z.X. Song, H. Zhao, Y. Xing, M. Zhao, J.G. Zhao, Z.A. Ma, P.P. Zhang, N. Tsubaki. Promotion of surface acidity and surface species of doped Fe and SO_4^{2-} over CeO_2 catalytic for NH_3-SCR reaction. Mol. Catal. 463 (2019) 1-7, https://doi.org/10.1016/j.mcat.2018.11.002.

[46] J.X. Mi, G.Q. Zhang, Q.Y. Zhang, W.T. Zhao, Y.N. Cao, F.J. Liu, L.L. Jiang. Defects modulating on MgAl-hydrotalcite nanosheet with improved performance in carbonyl sulfide elimination via a hydroxyl chemical looping route. Chem. Eng. Sci. 259 (2022) 117827, https://doi.org/10.1016/j.ces.2022.117827.

[47] M. Heidari, S.B. Mousavi, F. Rahmani, P.T. Clough, S. Ozmen. The novel Carbon Nanotube-assisted development of highly porous $CaZrO_3$-CaO xerogel with boosted sorption activity towards high-temperature cyclic CO_2 capture. Energ. Convers. Manage. 274 (2022) 116461, https://doi.org/10.1016/j.enconman.2022.116461.

[48] X.L. Tang, Y.R. Shi, F.Y. Gao, S.Z. Zhao, H.H. Yi, Z.L. Xie. Promotional role of Mo on $Ce_{0.3}FeO_x$ catalyst towards enhanced NH_3-SCR catalytic performance and SO_2 resistance. Chem. Eng. J. 398 (2020) 125619, https://doi.org/10.1016/j.cej.2020.125619.

[49] Z.H. Shen, X.D. Xing, S.X. Wang, M. Lv, J.K. Li, T. Li. Effect of K-Modified Blue Coke-Based Activated Carbon on Low Temperature Catalytic Performance of Supported Mn-Ce/Activated Carbon. ACS. Omega. 7 (2022) 8798-8807, https://doi.org/10.1021/acsomega.1c07076.

[50] Z.X. Song, Q.L. Zhang, P. Ning, J. Fan, Y.K. Duan, X. Liu, Z.Z. Huang. Effect of CeO_2 support on the selective catalytic reduction of NO with NH_3 over P-W/CeO_2. J. Taiwan. Inst. Chem. Eng. 65 (2016) 149-161, http://dx.doi.org/10.1016/j.jtice.2016.04.034.

[51] M.Y. Ma, C.M. Li, Y.J. Li, C. Wang, S.Q. Gao, H.D. Ye, J.J. Li, J. Yu. Resource Utilization of Spent Activated Coke as an Efficient Material for Simultaneous Removal of COS and H_2S. Energy. Fuel. 36 (2022) 4837-4846, https://doi.org/10.1021/acs.energyfuels.2c00325.

[52] Q.L. Zhang, J.H. Zhang, Z.X. Song, P. Ning, H. Li, X. Li. A novel and environmentally friendly SO_4^{2-}/CeO_2 catalyst for the selective catalytic reduction of NO with NH_3. J. Ind. Eng. Chem. 34 (2016) 165-171, http://dx.doi.org/10.1016/j.jiec.2015.11.006.

[53] G.Y. Mu, Y. Zeng, Y. Zheng, Y.N. Cao, F.J. Liu, S.J. Liang, Y.Y. Zhan, L.L. Jiang. Oxygen vacancy defects engineering on Cu-doped Co_3O_4 for promoting effective COS hydrolysis. Green. Energy. Environ. 8 (2023) 831-841, https://doi.org/10.1016/j.gee.2021.11.001.

[54] X.H. Zheng, Y.L. Li, L.Y. Zhang, L.J. Shen, Y.H. Xiao, Y.F. Zhang, C. Au, L.L. Jiang. Insight into the effect of morphology on catalytic performance of porous CeO_2 nanocrystals for H_2S selective oxidation. Appl. Catal. B 252 (2019) 98-110, https://doi.org/10.1016/j.apcatb.2019.04.014.

[55] B.M. Casaria, V. Langerb. New Structure Type among Octahydrated Rare-Earth Sulfates,

757 β-$Ce_2(SO_4)_3 \cdot 8H_2O$, and a new $Ce_2(SO_4)_3 \cdot 4H_2O$ Polymorph. Z. Anorg. Allg. Chem. 633 (2007) 1074-1081,
758 https://doi.org/10.1002/zaac.200700003.
759 [56] L. Chen, Y. Shen, Q.L. Wang, X.X. Wang, Y.Q. Wang, B.L. Li, S.J. Li, S.H. Zhang, W. Li. Phosphate on
760 ceria with controlled active sites distribution for wide temperature NH_3-SCR. J. Hazard. Mater. 427 (2022)
761 128148, https://doi.org/10.1016/j.jhazmat.2021.128148.
762 [57] W.X. Zou, C.Y. Ge, M.Y. Lu, S.G. Wu, Y.Z. Wang, J.F. Sun, Y. Pu, C.J. Tang, F. Gao, L. Dong. Engineering
763 the NiO/CeO_2 interface to enhance the catalytic performance for CO oxidation. RSC. Adv. 5 (2015) 98335,
764 https://doi.org/10.1039/C5RA20466F.
765 [58] S.J. Yi, P.C. Lai, G.L. Ma, J.J. Pan, Z. Chen, Y.H. Qin, X.M. Jiang. Green and facile synthesis of
766 nanostructured Co_3O_4/CeO_2 catalysts via a glucose-urea method for NO oxidation. Appl. Surf. Sci. 626
767 (2023) 157180, https://doi.org/10.1016/j.apsusc.2023.157180.
768 [59] R. Verma, S.K. Samdarshi, S. Bojja, S. Paul, B. Choudhury. A novel thermophoto catalyst of mixed-phase
769 cerium oxide (CeO_2/Ce_2O_3) homocomposite nanostructure: Role of interface and oxygen vacancies. Sol.
770 Energ. Mater. Sol. C 141 (2015) 414-422, http://dx.doi.org/10.1016/j.solmat.2015.06.027.
771 [60] L. Zhang, L. Zhang, G.C. Xu, C. Zhang, X. Li, Z.P. Sun, D.Z. Jia. Low-temperature CO oxidation over
772 CeO_2 and CeO_2@Co_3O_4 core-shell microspheres. New. J. Chem. 41 (2017) 13418,
773 https://doi.org/10.1039/C7NJ02542D.
774 [61] M. Jang, S. Choi, Y. Kim, J. Cha, A.R. Kim, H. Jeong, Y. Kim, S.H. Choi, S.W. Nam, J. Lim, C.W. Yoon, H.
775 Sohn. Effect of CeO_2 redox properties on the catalytic activity of Pt-CeO_x over irreducible SiO_2 support for
776 methylcyclohexane (MCH) dehydrogenation. Appl. Surf. Sci. 627 (2023) 157134,
777 https://doi.org/10.1016/j.apsusc.2023.157134.
778 [62] W. Tan, J.M. Wang, L.L. Li, A.N. Liu, G. Song, K. Guo, Y.D. Luo, F.D. Liu, F. Gao, L. Dong. Gas phase

779 sulfation of ceria-zirconia solid solutions for generating highly efficient and SO_2 resistant NH_3-SCR
780 catalysts for NO removal. J. Hazard. Mater. 388 (2020) 121729,
781 https://doi.org/10.1016/j.jhazmat.2019.121729.
782 [63] G.D. Zhang, X.S. Huang, Z.C. Tang. New insight into the synergistic promotion effect of phosphorus and
783 molybdenum on the ceria-titanium catalysts for superior SCR performance. Mol. Catal. 478 (2019) 110562,
784 https://doi.org/10.1016/j.mcat.2019.110562.
785 [64] X. Fang, Y.G. Liu, W.L. Cen, Y. Cheng. Birnessite as a Highly Efficient Catalyst for Low-Temperature
786 NH_3-SCR: The Vital Role of Surface Oxygen Vacancies. Ind. Eng. Chem. Res. 59 (2020) 14606-14615,
787 https://doi.org/10.1021/acs.iecr.0c00188.
788 [65] H.Z. Chang, L. Ma, S.J. Yang, J.H. Li, L. Chen, W. Wang, J.M. Hao. Comparison of preparation methods
789 for ceria catalyst and the effect of surface and bulk sulfates on its activity toward NH_3-SCR. J. Hazard.
790 Mater. 262 (2013) 782-788, http://dx.doi.org/10.1016/j.jhazmat.2013.09.043.
791 [66] A.C. Zhang, W.B. Xing, Z.H. Zhang, F.M. Meng, Z.C. Liu, J. Xiang, L.S. Sun. Promotional effect of SO_2
792 on CeO_2-TiO_2 material for elemental mercury removal at low temperature. Atmos. Pollut. Res. 7 (2016)
793 895-902, http://dx.doi.org/10.1016/j.apr.2016.05.003.
794 [67] M.D. Lane. Mid-infrared emission spectroscopy of sulfate and sulfate-bearing minerals. Am. Mineral. 92
795 (2007) 1-18, https://doi.org/10.2138/am.2007.2170.
796 [68] D.Q. An, S. Yang, W.X. Zou, J.F. Sun, W. Tan, J.W. Ji, Q. Tong, C.Z. Sun, D. Li, L. Dong. Unraveling the
797 SO_2 Poisoning Effect over the Lifetime of MeO_x (Me=Ce, Fe, Mn) Catalysts in Low-Temperature
798 NH_3-SCR: Interaction of Reaction Atmosphere with Surface Species. J. Phys. Chem. C 126 (2022)
799 12168-12177, https://doi.org/10.1021/acs.jpcc.2c02233.
800 [69] J. Li, H.S. Wu, B. Ma. Preparation of bimodal mesoporous silica containing cerious salt and its application

as catalyst for the synthesis of biodiesel by esterification. J. Porous. Mater. 24 (2017) 1279-1288, https://doi.org/10.1007/s10934-017-0368-3.

[70] P. Zhang, A.L. Chen, T.W. Lan, X.Y. Liu, T.T. Yan, W. Ren, D.S. Zhang. Balancing acid and redox sites of phosphorylated CeO_2 catalysts for NO_x reduction: The promoting and inhibiting mechanism of phosphorus. J. Hazard. Mater. 441 (2023) 129867, https://doi.org/10.1016/j.jhazmat.2022.129867.

[71] S.J. Hu, J.N. Gu, K. Li, J.X. Liang, Y.X. Xue, X. Min, M.M. Guo, X.F. Hu, J.P. Jia, T.H. Sun. Boosting COS catalytic hydrolysis performance over Zn-Al oxide derived from ZnAl hydrotalcite-like compound modified via the dopant of rare earth metals and the replacement of precipitation base. Appl. Surf. Sci. 599 (2022) 154016, https://doi.org/10.1016/j.apsusc.2022.154016.

[72] S. Gao, X.B. Chen, H.Q. Wang, J.S. Mo, Z.B. Wu, Y. Liu, X.L. Weng. Ceria supported on sulfated zirconia as a superacid catalyst for selective catalytic reduction of NO with NH_3. J. Colloid. Interf. Sci. 394 (2013) 515-521, http://dx.doi.org/10.1016/j.jcis.2012.12.034.

[73] H.P. Pang, Z.H. Shen, X.D. Xing. Removal of CO from sintering flue gas by CuO-CeO_2 catalyst supported on $KMnO_4$ modified activated carbon. Clean. Coal. Technol. 29 (2023) 63-68, http://dx.doi.org/10.13226/j.issn.1006-6772.22100601.

[74] A. Younis, D.W. Chu, Y.V. Kaneti, S.A. Li. Tuning the surface oxygen concentration of {111} surrounded ceria nanocrystals for enhanced photocatalytic activities. Nanoscale. 8 (2016) 378, https://doi.org/10.1039/C5NR06588G.

[75] Y. Li, S.X. Cai, P.L. Wang, T.T. Yan, J.P. Zhang, D.S. Zhang. Improved NO_x Reduction over Phosphate-Modified Fe_2O_3/TiO_2 Catalysts Via Tailoring Reaction Paths by In Situ Creating Alkali-Poisoning Sites. Environ. Sci. Technol. 55 (2021) 9276-9284, https://doi.org/10.1021/acs.est.1c01722.

[76] L. Huang, Y.W. Yue, Y.H. Zong, J.K. Li, Y.B. Gao, H. Wang, P. Han. Effect of impregnation sequence of vanadium and molybdenum on the Na resistance of de-NO_x catalyst. Clean. Coal. Technol. 29 (2023) 74-79, https://doi.org/10.13226/j.issn.1006-6772.22051703.

[77] L. Huang, Y.Q. Zeng, Z.F. Chang, Y.H. Zong, H. Wang, S.L. Zhang, Y. Yu. Promotional effect of phosphorus modification on improving the Na resistance of V_2O_5-MoO_3/TiO_2 catalyst for selective catalytic reduction of NO_x by NH_3. Mol. Catal. 506 (2021) 111565, https://doi.org/10.1016/j.mcat.2021.111565.

[78] S.H. Wang, C. Fan, Z.Q. Zhao, Q. Liu, G. Xu, M.H. Wu, J.J. Chen, J.H. Li. A facile and controllable in situ sulfation strategy for CuCeZr catalyst for NH_3-SCR. Appl. Catal. A 597 (2020) 117554, https://doi.org/10.1016/j.apcata.2020.117554.

[79] M.Y. Guo, Q.L. Liu, P.P. Zhao, J.F. Han, X. Li, Y. Ha, Z.C. Fu, C.F. Song, N. Ji, C.X. Liu, D.G. Ma, Z.G. Li. Promotional effect of SO_2 on Cr_2O_3 catalysts for the marine NH_3-SCR reaction. Chem. Eng. J. 361 (2019) 830-838, https://doi.org/10.1016/j.cej.2018.12.100.

[80] Y.Y. Peng, L. Song, S.R. Lu, Z.Y. Su, K. Ma, S.Y. Tang, S. Zhong, H.R. Yue, B. Liang. Superior resistance to alkali metal potassium of vanadium-based NH_3-SCR catalyst promoted by the solid superacid SO_4^{2-}-TiO_2. Chinese. J. Chem. Eng. 55 (2023) 246-256, https://doi.org/10.1016/j.cjche.2022.05.031.

[81] X. Sun, P. Ning, X.L. Tang, H.H. Yi, K. Li, D. He, X.M. Xu, B. Huang, R.Y. Lai. Simultaneous catalytic hydrolysis of carbonyl sulfide and carbon disulfide over Al_2O_3-K/CAC catalyst at low temperature. J. Energy Chem. 23 (2014) 221-226, https://doi.org/10.1016/S2095-4956(14)60139-X.

[82] L. Zhang, L.L. Li, Y. Cao, X.J. Yao, C.Y. Ge, F. Gao, Y. Deng, C.J. Tang, L. Dong. Getting insight into the influence of SO_2 on TiO_2/CeO_2 for the selective catalytic reduction of NO by NH_3. Appl. Catal. B 165 (2015) 589-598, https://doi.org/10.1016/j.apcatb.2014.10.029.

[83] P. Zhang, R.T. Guo, L.J. Wu, W.G. Pan. The enhancement of NH_3-SCR performance for CeO_2 catalyst by CO pretreatment. Environ. Sci. Pollut. R. 27 (2020) 13617-13636, https://doi.org/10.1007/s11356-020-07908-z.

[84] S.Y. Xu, L.T. Yin, H.M. Wang, L.Y. Gao, X.Y. Tian, J.J. Chen, Q.L. Zhang, P. Ning. Improved alkali-tolerance of FeO_x-WO_3 catalyst for NO removal via in situ reserving FeO_x active species. Sep. Purif. Technol. 300 (2022) 121824, https://doi.org/10.1016/j.seppur.2022.121824.

[85] C. Fang, L.Y. Shi, H.R. Li, L. Huang, J.P. Zhang, D.S. Zhang. Creating hierarchically macro-/mesoporous Sn/ CeO_2 for the selective catalytic reduction of NO with NH_3. RSC. Adv. 6 (2016) 78727, https://doi.org/10.1039/C6RA18339E.

[86] D.S. Zhang, L. Zhang, L.Y. Shi, C. Fang, H.R. Li, R.H. Gao, L. Huang, J.P. Zhang. In situ supported MnO_x-CeO_x on carbon nanotubes for the low-temperature selective catalytic reduction of NO with NH_3. Nanoscale. 5 (2013) 1127, https://doi.org/10.1039/C2NR33006G.

[87] J.J. Jin, Z.X. Song, X.J. Zhang, Y.L. Mao. Role of silicotungstic acid on the catalytic performance over CeO_2-HSiW catalysts for selective catalytic reduction of NO_x with NH_3. Appl. Organomet. Chem. 35 (2021) e6237, https://doi.org/10.1002/aoc.6237.

[88] L.F. Jia, J.X. Liu, D.Q. Huang, J.C. Zhao, J.N. Zhang, K.X. Li, Z.G. Li, W.S. Zhu, Z. Zhao, J. Liu. Interface Engineering of a Bifunctional Cu-SSZ-13@CZO Core-Shell Catalyst for Boosting Potassium Ion and SO_2 Tolerance. ACS. Catal. 12 (2022) 11281-11293, https://doi.org/10.1021/acscatal.2c03048.

[89] X. Song, P. Ning, C. Wang, K. Li, L.H. Tang, X. Sun. Catalytic hydrolysis of COS over CeO_2 (110) surface: A density functional theory study. Appl. Surf. Sci. 414 (2017) 345-352, http://dx.doi.org/10.1016/j.apsusc.2017.04.119.

[90] Z. Wei, M.F. Zhao, Z.W. Yang, X.X. Duan, G.X. Jiang, G.G. Li, F.L. Zhang, Z.P. Hao. Oxygen

867 vacancy-engineered titanium-based perovskite for boosting H_2O activation and lower-temperature
868 hydrolysis of organic sulfur. P. Natl. A. Sci. 120 (2023) e2217148120,
869 https://doi.org/10.1073/pnas.2217148120.